# SUPPLEMENTAL MATERIALS

ASCE *Journal of Water Resources Planning and Management*

# Bias Correction of Hydrologic Projections Strongly Impacts Inferred Climate Vulnerabilities in Institutionally Complex Water Systems

Keyvan Malek, Patrick Reed, Harrison Zeff, Andrew Hamilton, Melissa Wrzesien, Natan Holtzman, Scott Steinschneider, Jonathan Herman, and Tamlin Pavelsky

**DOI:** 10.1061/(ASCE)WR.1943-5452.0001493

## Contents of this file

## Introduction

The Supplemental Materials provides a more comprehensive description of the simulation tools and methods used in this study. Also, the document includes more information about the performance of our baseline scenarios as well as limitations of the study. Finally, this document presents additional results that support and augment the main contributions of the study.

### Note S1. Baseline Errors for CALFEWS

In this study, we assess the accuracy of the CALFEWS model by comparing the simulation to historical observations for three critical components of the California water system: water volume stored behind dams (Figure S3 and S4, and Table S1), dam releases (Figure S3 and S4, and Table S2), and pumped water deliveries through the Sacramento-San Joaquin Delta (Figure 2 in the main body of the manuscript, and Table S3). Our results indicate that the baseline historical CALFEWS simulation (CFEWS-HIS) can reasonably capture the complex dynamics of the infrastructure systems and their operations. Accuracy deteriorates under the other simulated streamflow scenarios (CGW, NGW, and BC). For example, the Nash-Sutcliff efficiencies Nash and Sutcliffe Efficiency (NSE , Nash and Sutcliffe 1970, ideal value 1.0) of the CALFEWS simulation of daily water storage behind the Shasta dam were 0.92, 0.68, 0.20, and 0.21 for the CFEWS-HIS, CGW, NGW, and BC streamflow inputs, respectively (Table S1). Simulated outflow from the other main reservoirs of the system showed similar patterns of performance (Table S2). In addition, our baseline (CFEWS-HIS) simulations for pumping to the SWP were 0.68, 0.32, 0.26, and 0.36 for the CFEWS-HIS, CGW, NGW, and BC inputs, respectively (Table S3). Although CALFEWS itself as a model is subject to imperfections in its underlying data and processes (Oreskes et al. 1994), it is unique in its ability to simulate daily time-scale infrastructure dynamics coupled to their financial implications for irrigation districts in the Central Valley. In this study, we consider CALFEWS simulations under observed streamflow (CFEWS-HIS) as our best-available modeling baseline for the institutionally complex water balance dynamics of the system. A more comprehensive performance assessment of various components of CALFEWS is presented in (Zeff et al. 2020).

### Note S2. Performance Metrics of Input Streamflow to Reservoirs

We compare the simulated streamflow with the observed streamflow (Section 2.1 in the main body of the manuscript and Table S4). Our performance metrics are Mean Error (ME), Mean Absolute Error (MAE), Root Mean Square Error (RMSE), and Nash-Sutcliffe

Efficiency (NSE). The following equations were used to calculate these performance metrics:

$$ME = \frac{1}{N}\sum_{i=1}^{N}(S_i - O_i) \quad (1)$$

$$MAE = \frac{1}{N}\sum_{i=1}^{N}|(S_i - O_i)| \quad (2)$$

$$RMSE = \sqrt{\frac{1}{N}\sum_{i=1}^{N}(S_i - O_i)^2} \quad (3)$$

$$NSE = 1 - \frac{\sum_{i=1}^{N}(S_i - O_i)^2}{\sum_{i=1}^{N}(O_i - \overline{O})^2} \quad (4)$$

where, $S_i$ is the simulated streamflow in day; $O_i$ is the observed streamflow in day I; $N$ is the number of records; and $\overline{O}$ is the average streamflow over all records. These error metrics reveal specific types of information about the performance of our hydrologic models (Gupta et al. 1998, 2008). For example, *RMSE* tends to focus on misrepresentations of high-flow events, and *ME* gives an equal weight to all the error types during wet and dry periods.

**Note S3. Quantile Mapping-Based Bias Correction**

Statistical bias correction has been widely used by hydrologic and atmospheric science community to ameliorate the errors included in model simulated states and fluxes such as precipitation, temperature, and streamflow. Various methods that have been proposed to reduce the effect of these errors. For example, there are simple nudging and impact factor methods (Hawkins et al. 2013; Luo et al. 2018) that have been mainly used to match the average of model simulated time series with observed. There are also parametric or non-parametric distribution-based quantile mapping methods that can improve higher moments of the time series (Cannon et al. 2015; Maraun 2013). In essence, bias correction is a statistical transformation (Piani et al. 2010) that makes model simulations ($X_m$) statistically consistent with historical observations ($X_o$):

$$X_m^{bc} = f(X_m)$$

In distribution-based methods the following relationship can describe the overall mathematical relationship between model simulated, observed and bias corrected time series (Gudmundsson et al. 2012; Mishra et al. 2020):

$$X_m^{bc} = F_o^{-1}\big(F_m(X_m)\big)$$

Atmospheric science research community have also developed more sophisticated bias-correction methods that simultaneously bias correct closely correlated parameters such as precipitation and temperature (Cannon 2018; Cannon et al. 2015; François et al. 2020; Luo et al. 2018; Maraun 2013). However, single variate quantile mapping approaches

have remained the most prevalent bias-correction method among the hydrologists for improvement of model simulated streamflow.

In this study, we used a popular statistical bias-correction technique called quantile mapping to remove systematic biases of raw WRF-Noah-MP streamflow data. To do this, we developed and used an R package called "biascorrection" that follows the methodology described by Hamlet and Lettenmaier (1999). In short, the bias correction module uses the historical observed streamflow to create the monthly flow quantiles of each individual month. After that, it uses the simulated streamflow data to create simulated monthly flow quantiles. Afterwards, the bias correction module creates the monthly bias-corrected flow by swapping each month of the simulated flow with the same quantile from the observed streamflow. Since hydrologic models can simulate the average annual flow reasonably well, after constructing the monthly bias-corrected flow, we adjust them to make sure that their average annual flow is consistent with what the WRF-Noah-MP model has simulated. Finally, we disaggregate the monthly bias-corrected flow to daily by multiplying the raw daily simulated flow of each month by the simulated bias-corrected ratio of that month. Figure S23 shows how the quantile mapping bias correction affect the simulated WRF-Noah-MP streamflow to Shasta Dam. In short, the bias correction process tends to improve the quality of simulation during low-flow periods while creating systematic underestimation tendency during high-flow periods. The package can be downloaded from GitHub (https://github.com/keyvan-malek/biascorrection). In addition, the following blog post (https://waterprogramming.wordpress.com/2020/09/15/introducing-the-r-package-biascorrection/) provides more technical detail about the "*biascorrection*" module.

**Note S4. Water Price Scenarios**

To plausibly estimate revenue effects for different irrigation districts, we have generated 100 synthetic water price scenarios (Figure S15). A synthetic water price dataset is required because at present there are no publicly available databases with detailed temporal water pricing for all 25 simulated irrigation districts considered over our period of analysis. Drawing on the water rate timeseries of the Semitropic Irrigation district as the plausible baseline scenario, it serves to support the generation of the rest of our synthetic time series. Our analysis indicate that California has been experiencing an overall increasing trend of inflation adjusted water price (Figure S15 – Panel a). Previous studies of water price in California argue that the aging infrastructures and the more-frequent droughts in recent years have made water utilities less financially stable and have contributed to this increasing trend for water rates (Donnelly and Christian-Smith 2013; Wallis-Lage and Chevrette 2012; Wichelns 2010). We implemented the following procedure to generate our synthetic pricing scenarios:

First, we defined 5 baseline water price rate scenarios. These baseline scenarios represent different plausible ranges of water price fluctuations during California's drought years (i.e., 2007, 2008, 2009, 2013, 2014, and 2015). We focus on drought years because these periods are the most uncertain times in terms of changing water rates (Medellín-Azuara et al. 2012). Our first scenario (Scenario 1) represents a condition that water price declines by 25% during the drought years. Scenario 2 identically follows the water rate trajectory of our observed Semitropic water rate timeseries. The last three scenarios (Scenarios 3, 4 and 5) represent the condition that water rate increases during drought years. More specifically, in Scenario 3, Scenario 4, and Scenario 5 water rate increases by 20%, 50%, and 80%, respectively. The price increase is the most likely direction of price change during drought years (Howitt et al. 2014; Medellín-Azuara et al. 2012), which tends to encourage water conservation and improves the revenue of districts (Mitchell et al. 2017). Our analysis in this study (Figure S15 – Panel b) also demonstrates that water price is likely to increase with aggravated supply shortages. The purpose of our water pricing scenarios is not meant to be predictive, but instead to provide a wide exploratory envelope for discovering consequential outcomes (Moallemi et al. 2020).

Second, we assigned a range of variability (10%) to all simulation scenarios. For all years, we assumed that the standard deviation of water price equals ten percent of the average value of each water price scenario during that year. This additional source of pricing variation adds stochasticity to the baseline observations, and better represents how prices can vary on weekly basis in the real world. As Figure S15 – Panel d indicates, this synthetic scenario generation approach allows us to consider a broad range of plausible water prices. Also, we assume that water prices in different years follow a normal distribution. We test this assumption (Figure S15 – Panel c) and show that the distribution of inflation-adjusted water price during different years falls within the 95% confidence interval of the theoretical quantiles of a normal distribution. Therefore, we used the standard deviation and average water price of each baseline water rate scenario and drew 100 samples for each year (20 per scenario), and created one hundred 10-year realization of water price for Semitropic irrigation district (Figure 15 – Panel d). Third, we use the 100 water price time series that we developed for Semitropic (Figure S15 – Panel d) to generate water price scenarios of other irrigation districts. To do that we multiplied each of the Semitropic's water price time series by the ratio of the average price in each irrigation district and Semitropic. We also compared our baseline water rate timeseries against a recorded annual water price time series obtained through personal communication with the Lower Tule irrigation district (Figure S15 – Panel a). However, the dataset did not include water prices during the years 2014 and 2015. However, because our baseline price rate timeseries (i.e., Semitropic) was similar to Lower Tule's time series, we used Lower Tule's 2016 water rate to fill the missing value of our baseline scenario during the year 2016.

**Note S5. Study Limitations**

Although our water management model, CALFEWS, has been carefully evaluated in its ability to simulate hundreds of water structures as well as sophisticated operational decisions and institutional relationships, we do acknowledge that our results inevitably suffer from a degree of uncertainty stemming from structural imperfections. Likewise, this study concentrates on a subset of key components of the north-central California water system, namely, major reservoirs, pumping to CVP and SWP, groundwater banks, and irrigation districts, but there are other system components that CALFEWS simulates and we do not investigate here, such as delta outflow, environmental flow requirements, and the detailed systems of southern California. However, we do not expect that taking account of these limitations would fundamentally modify our conclusions about the effects of errors on the key agro-hydrologic components of the system.

# Supplementary Figures

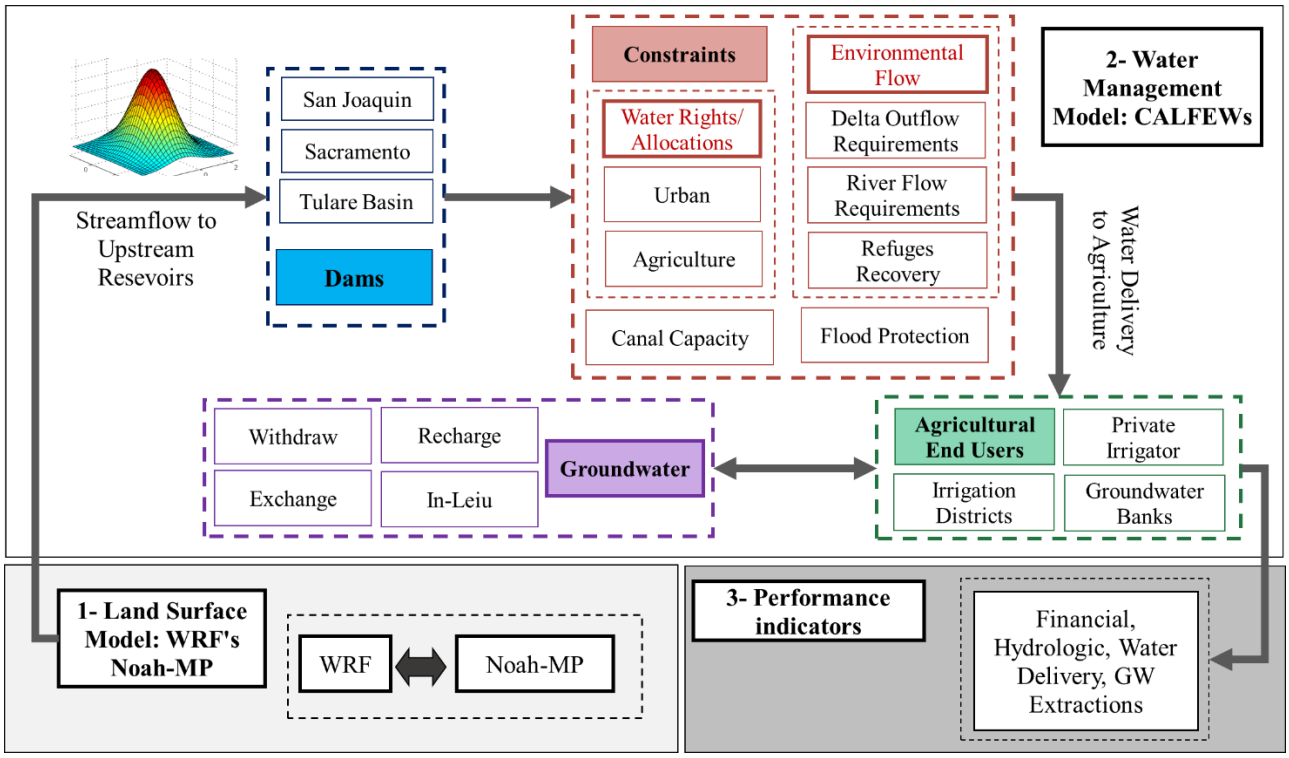


**Figure S1.** Modeling framework used in this study. Panel-1 shows the atmospheric and land-surface components of the modeling framework. Panel-2 illustrates the CALFEWS water management model and summary of its main components and operational considerations. Panel-3 indicates a few of the indicator generated from CALFEWS.

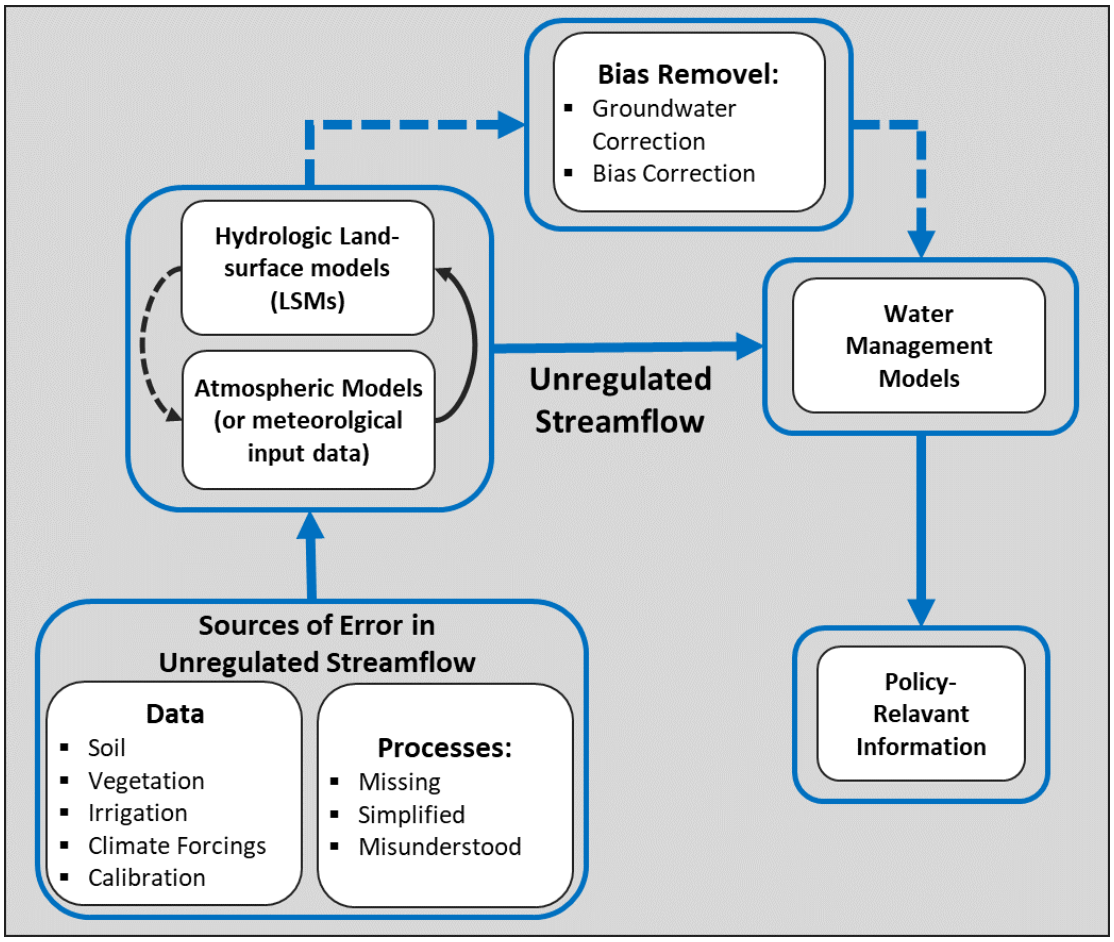


**Figure S2.** A generic integrated water systems simulation platform that is typically used in water resources planning and vulnerability assessment studies. Dashed-lines indicate components that are not always present in these platforms.

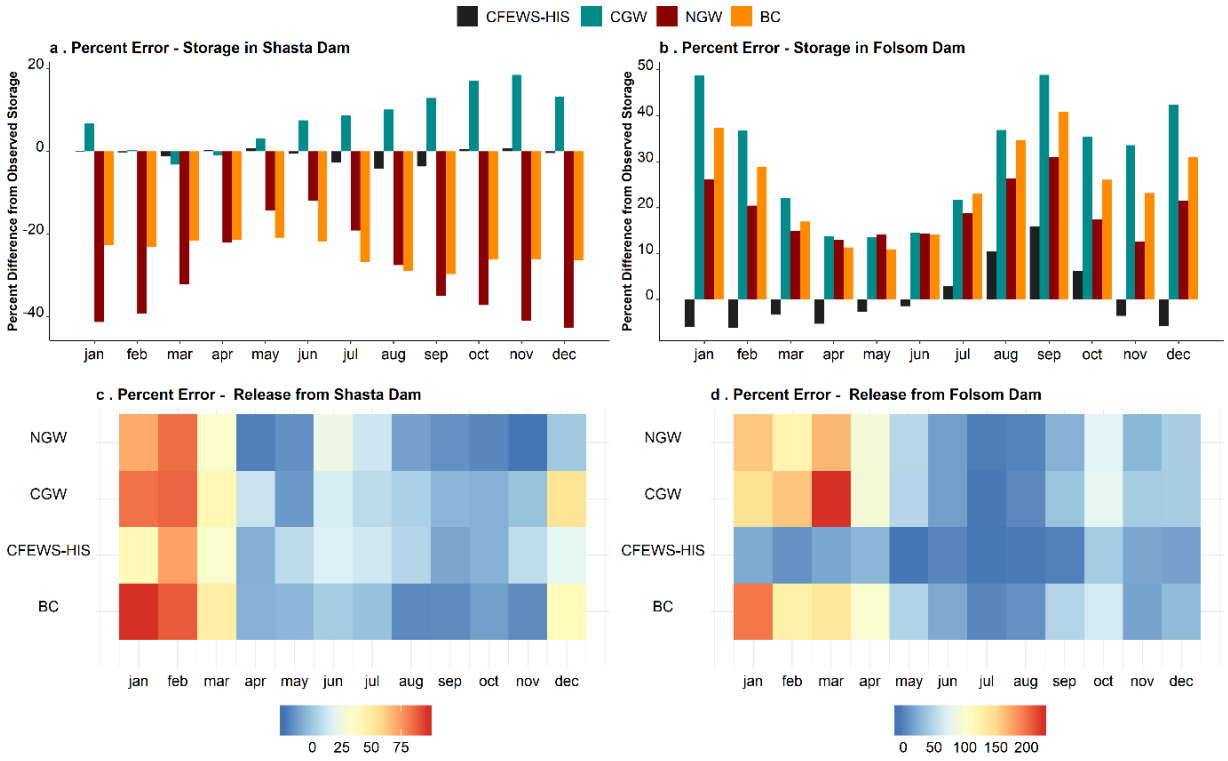


**Figure S3.** Evaluation of CALFEWS performance under different streamflow scenarios. Panel a and b show observed vs. CALFEWS-simulated water storage behind two major dams in California (i.e., Shasta and Folsom). Panel c and d compare recorded vs. simulated reservoir outflow from Shasta and Folsom. The simulated scenarios include CALFEWS under the following four streamflow input datasets: i) observed flow from California Department of Water Resources' Data Exchange Center (CFEWS-HIS), ii) raw WRF-Noah-MP (NGW), iii) groundwater corrected WRF-Noah-MP (CGW), and iv) bias-corrected WRF-Noah-MP (CGW). In this figure percent error is calculated through dividing the difference between each scenario and observed records by the observed records. More information about the error metrics is presented in the Supplemental Materials. Also, errors were calculated for the daily time steps and aggregated over each month.

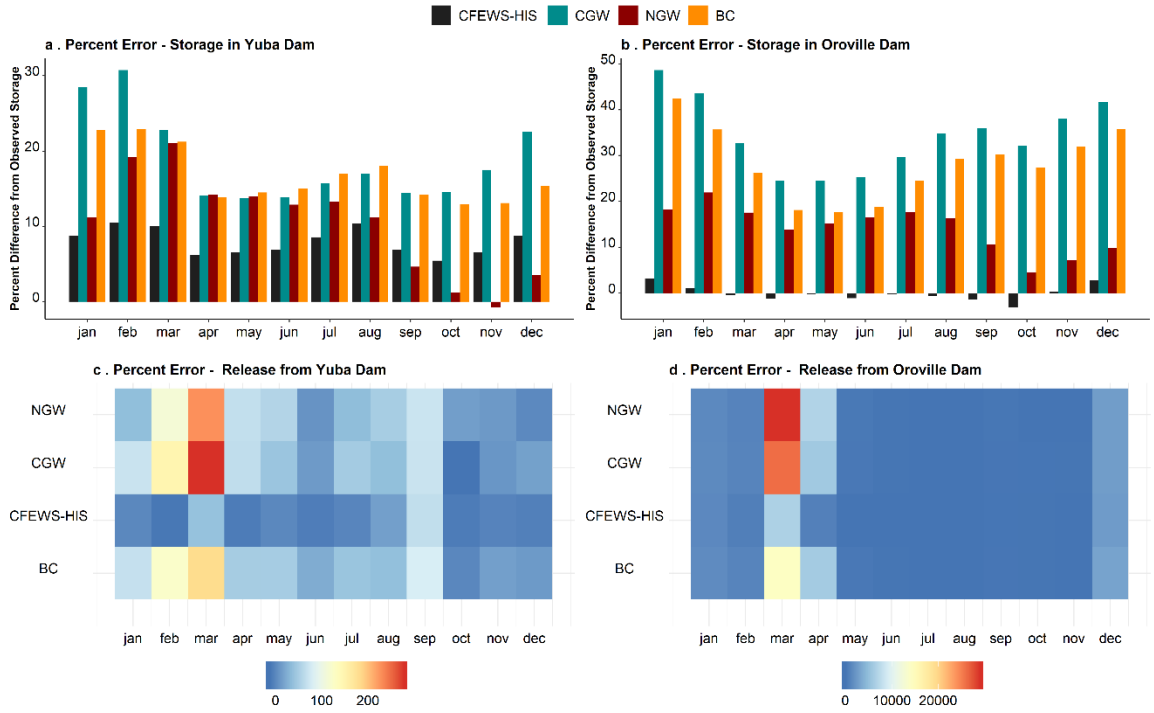


**Figure S4.** Evaluation of CALFEWs performance under different streamflow scenarios. Panel a and b show observed vs. CALFEWs-simulated water storage behind two major dams in California (i.e., Yuba and Oroville). Panel c and d compare recorded vs. simulated reservoir outflow from Yuba and Oroville. The simulated scenarios include CALFEWs under the following four streamflow input datasets: i) observed flow from California Department of Water Resources' Data Exchange Center (CDEC), ii) raw WRF-Noah-MP (NGW), iii) groundwater corrected WRF-Noah-MP (CGW), and iv) bias-corrected WRF-Noah-MP (CGW). In this figure percent error is calculated through dividing the difference between each scenario and observed records by the observed records. More information about the error metrics is presented in the Supplementary Note 5. Also, errors where calculated for the daily time steps and aggregated over each month.

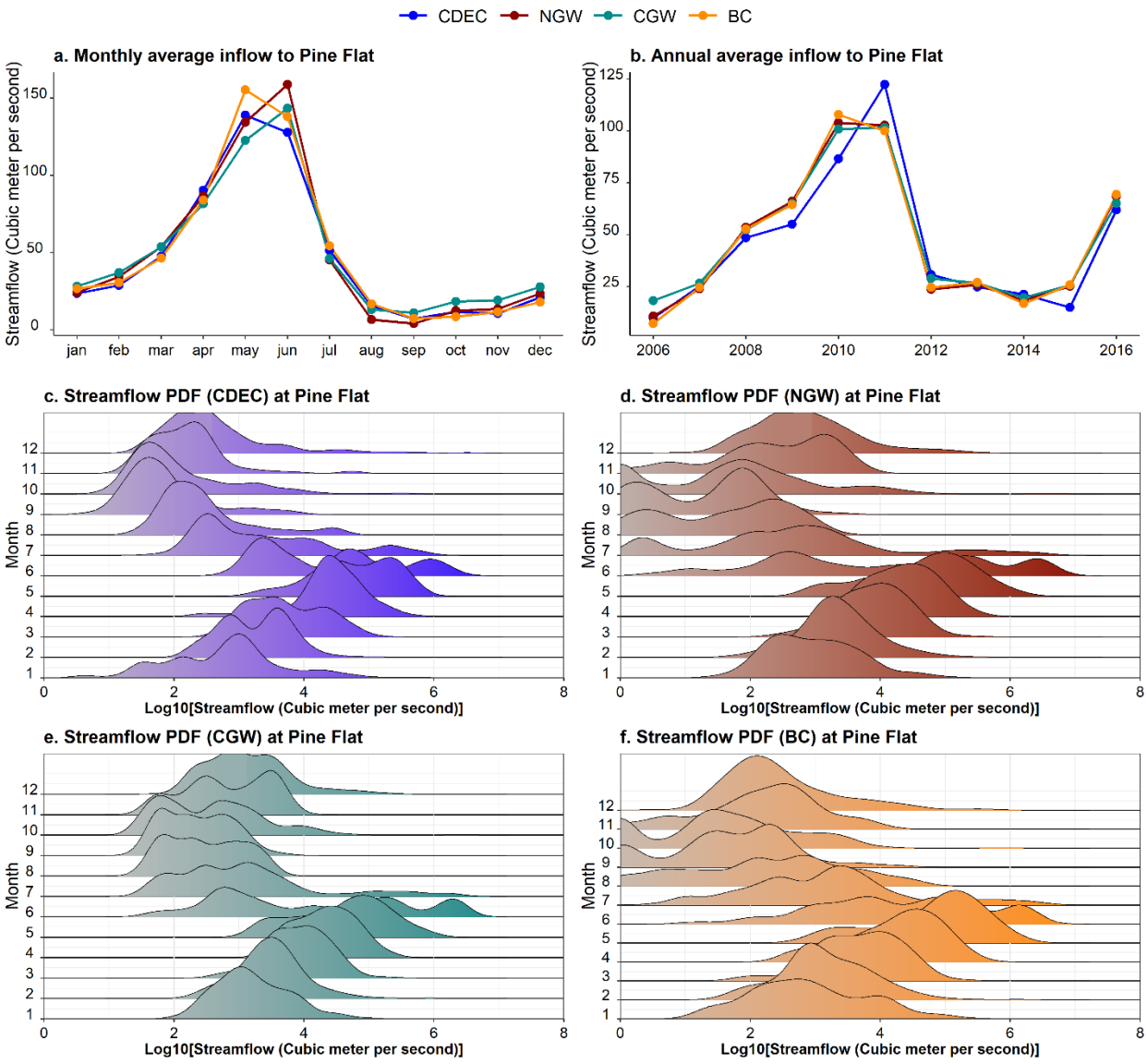


**Figure S5.** Comparison between the observed and simulated streamflow scenarios at Pine Flat Dam. The simulated streamflow scenarios include raw WRF-Noah-MP flow (NGW), WRF Noah-MP groundwater-corrected flow (CGW), and bias-corrected flow (BC). Panel a. and b. demonstrate the average monthly and average annual streamflow, respectively. Panel c., d., e., and f. show the monthly separated probability density function of daily streamflow for our four flow scenarios (observed, groundwater corrected, no groundwater correction, and bias-corrected).

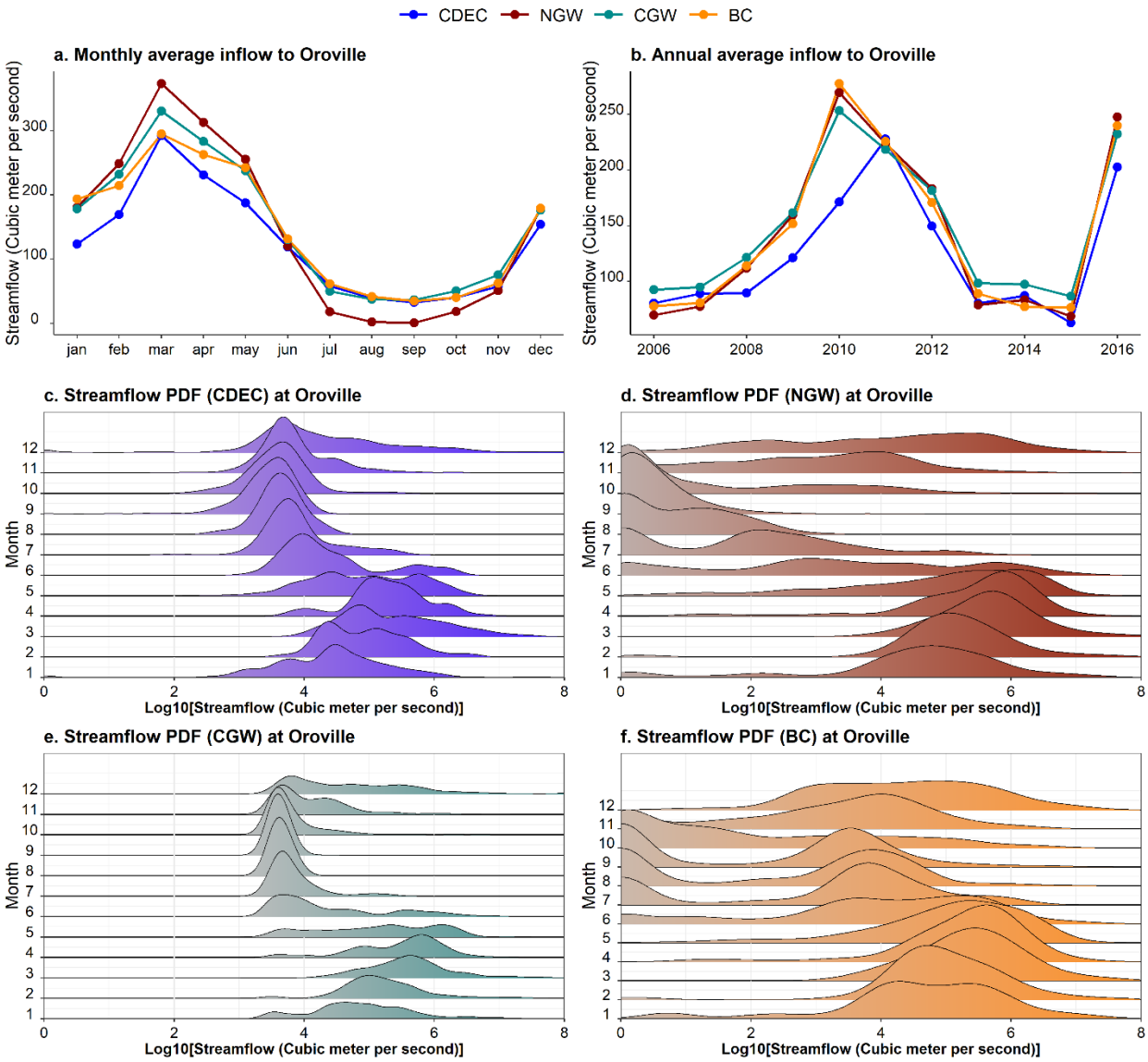


**Figure S6.** Comparison between the observed and simulated streamflow scenarios at Oroville Dam. The simulated streamflow scenarios include raw WRF-Noah-MP flow (NGW), WRF Noah-MP groundwater-corrected flow (CGW), and bias-corrected flow (BC). Panel a. and b. demonstrate the average monthly and average annual streamflow, respectively. Panel c., d., e., and f. show the monthly separated probability density function of daily streamflow for our four flow scenarios (observed, groundwater corrected, no groundwater correction, and bias-corrected).

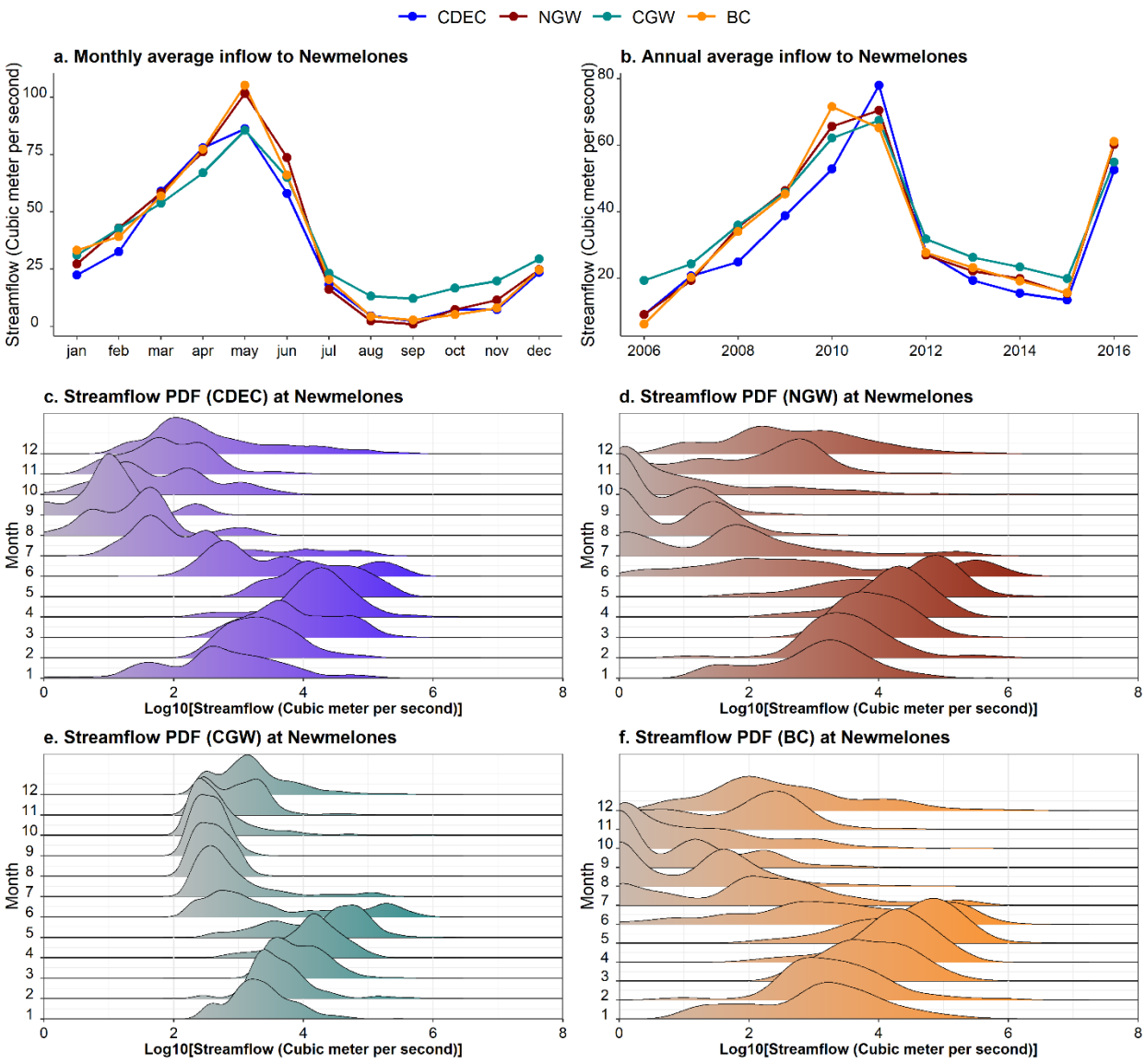


**Figure S7.** Comparison between the observed and simulated streamflow scenarios at New Melones Dam. The simulated streamflow scenarios include raw WRF-Noah-MP flow (NGW), WRF Noah-MP groundwater-corrected flow (CGW), and bias-corrected flow (BC). Panel a. and b. demonstrate the average monthly and average annual streamflow, respectively. Panel c., d., e., and f. show the monthly separated probability density function of daily streamflow for our four flow scenarios (observed, groundwater corrected, no groundwater correction, and bias-corrected).

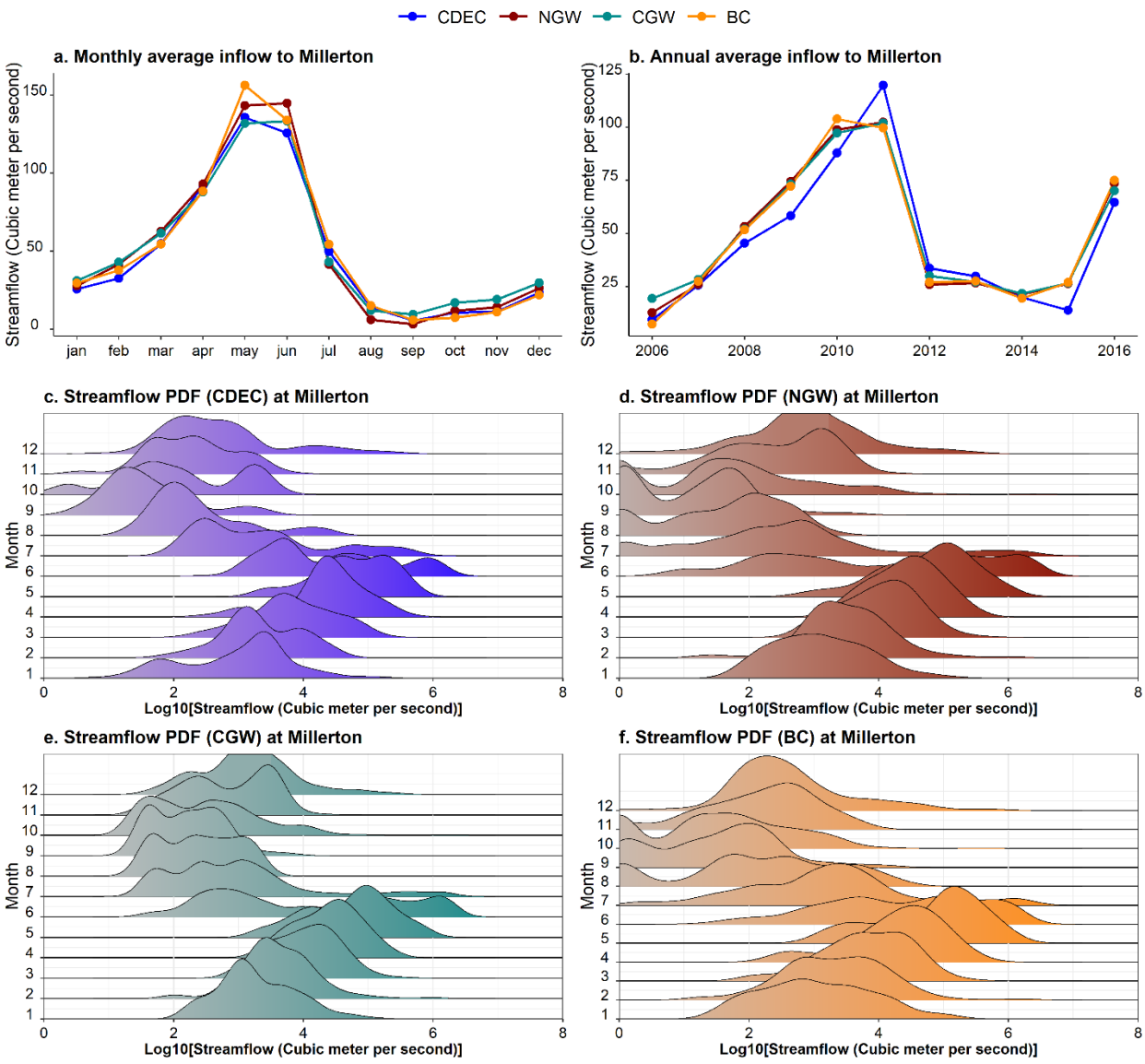


**Figure S8.** Comparison between the observed and simulated streamflow scenarios at Millerton Dam. The simulated streamflow scenarios include raw WRF-Noah-MP flow (NGW), WRF Noah-MP groundwater-corrected flow (CGW), and bias-corrected flow (BC). Panel a. and b. demonstrate the average monthly and average annual streamflow, respectively. Panel c., d., e., and f. show the monthly separated probability density function of daily streamflow for our four flow scenarios (observed, groundwater corrected, no groundwater correction, and bias-corrected).

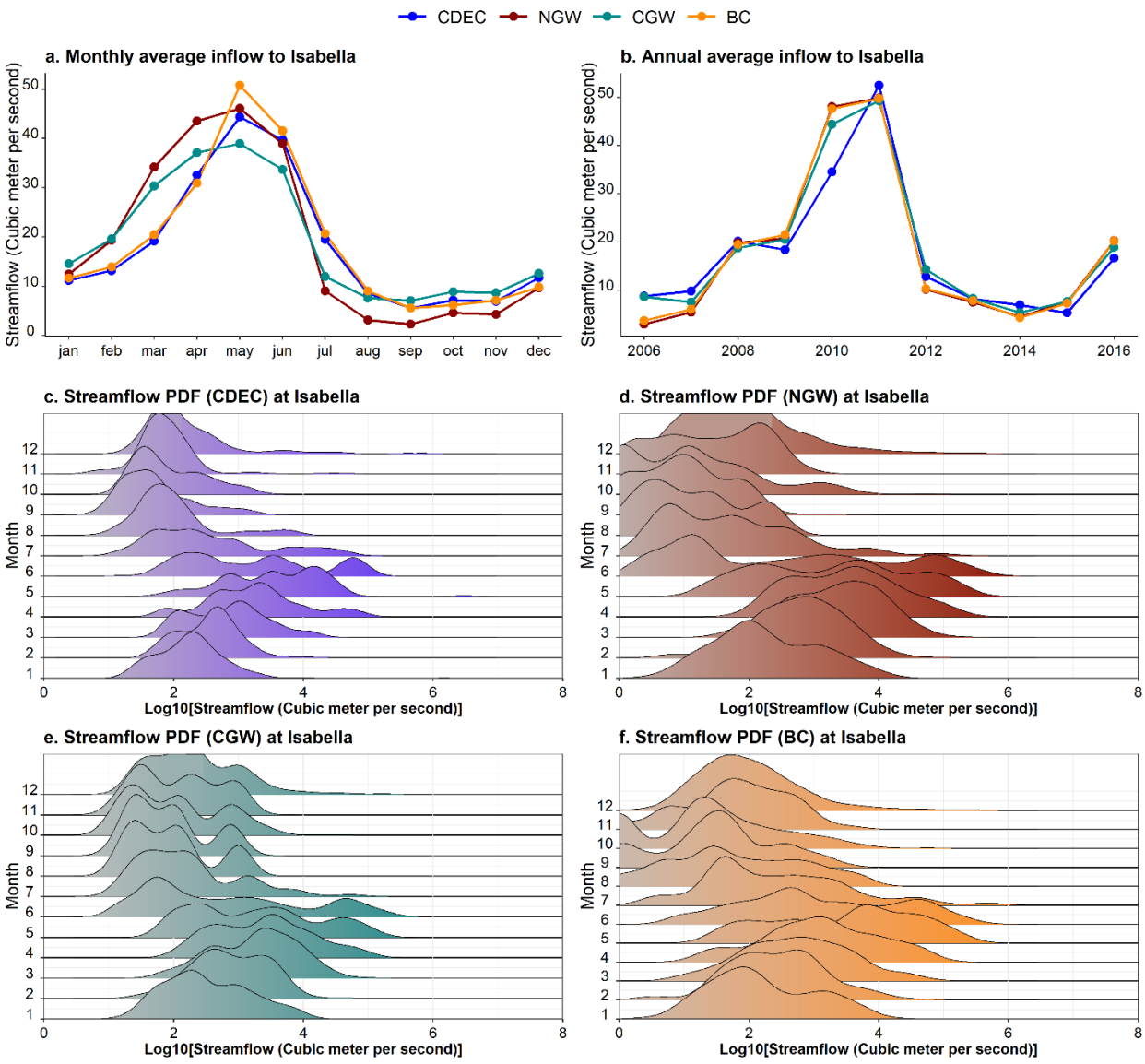


**Figure S9.** Comparison between the observed and simulated streamflow scenarios at Isabella Dam. The simulated streamflow scenarios include raw WRF-Noah-MP flow (NGW), WRF Noah-MP groundwater-corrected flow (CGW), and bias-corrected flow (BC). Panel a. and b. demonstrate the average monthly and average annual streamflow, respectively. Panel c., d., e., and f. show the monthly separated probability density function of daily streamflow for our four flow scenarios (observed, groundwater corrected, no groundwater correction, and bias-corrected).

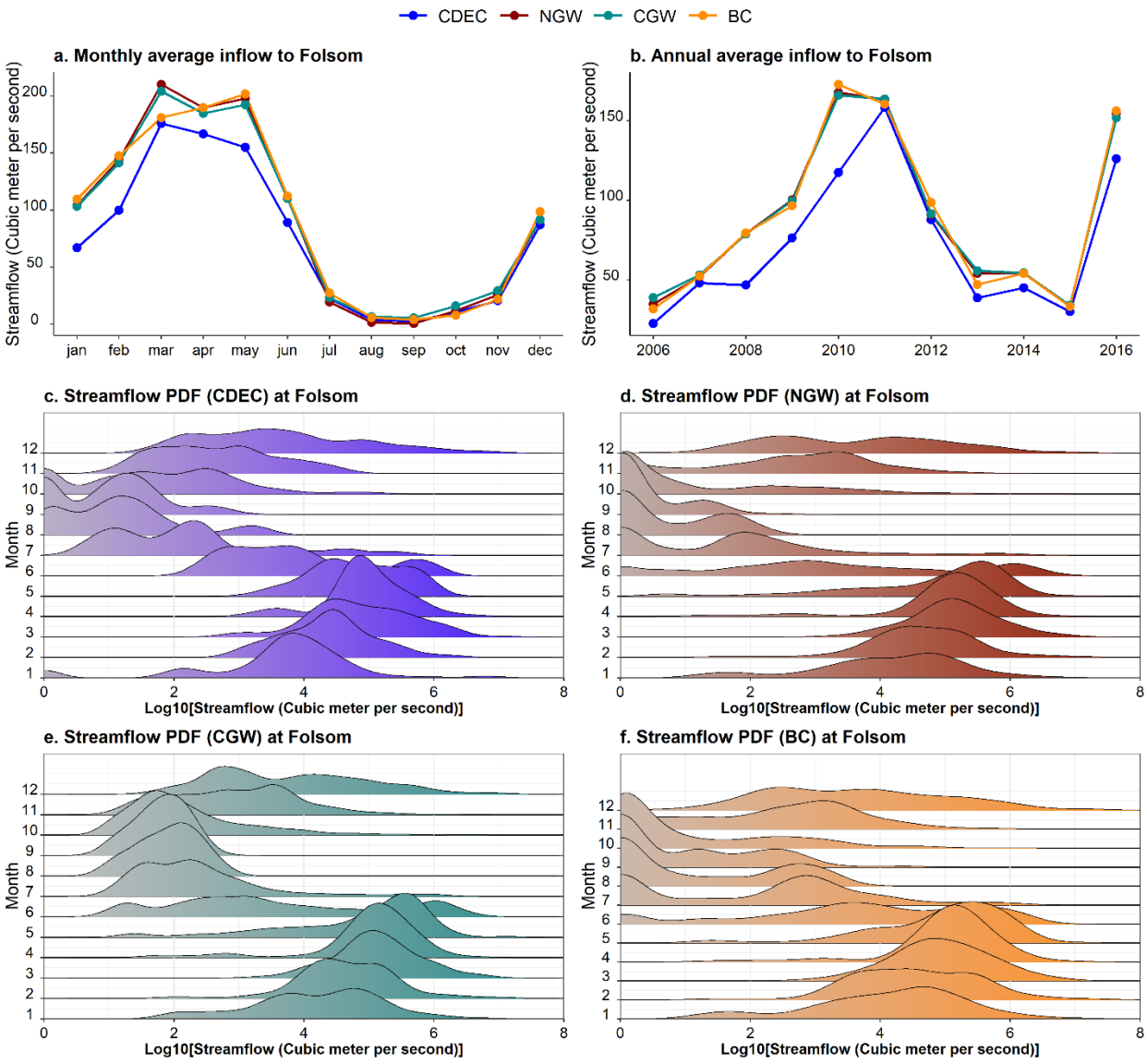


**Figure S10.** Comparison between the observed and simulated streamflow scenarios at Folsom Dam. The simulated streamflow scenarios include raw WRF-Noah-MP flow (NGW), WRF Noah-MP groundwater-corrected flow (CGW), and bias-corrected flow (BC). Panel a. and b. demonstrate the average monthly and average annual streamflow, respectively. Panel c., d., e., and f. show the monthly separated probability density function of daily streamflow for our four flow scenarios (observed, groundwater corrected, no groundwater correction, and bias-corrected).

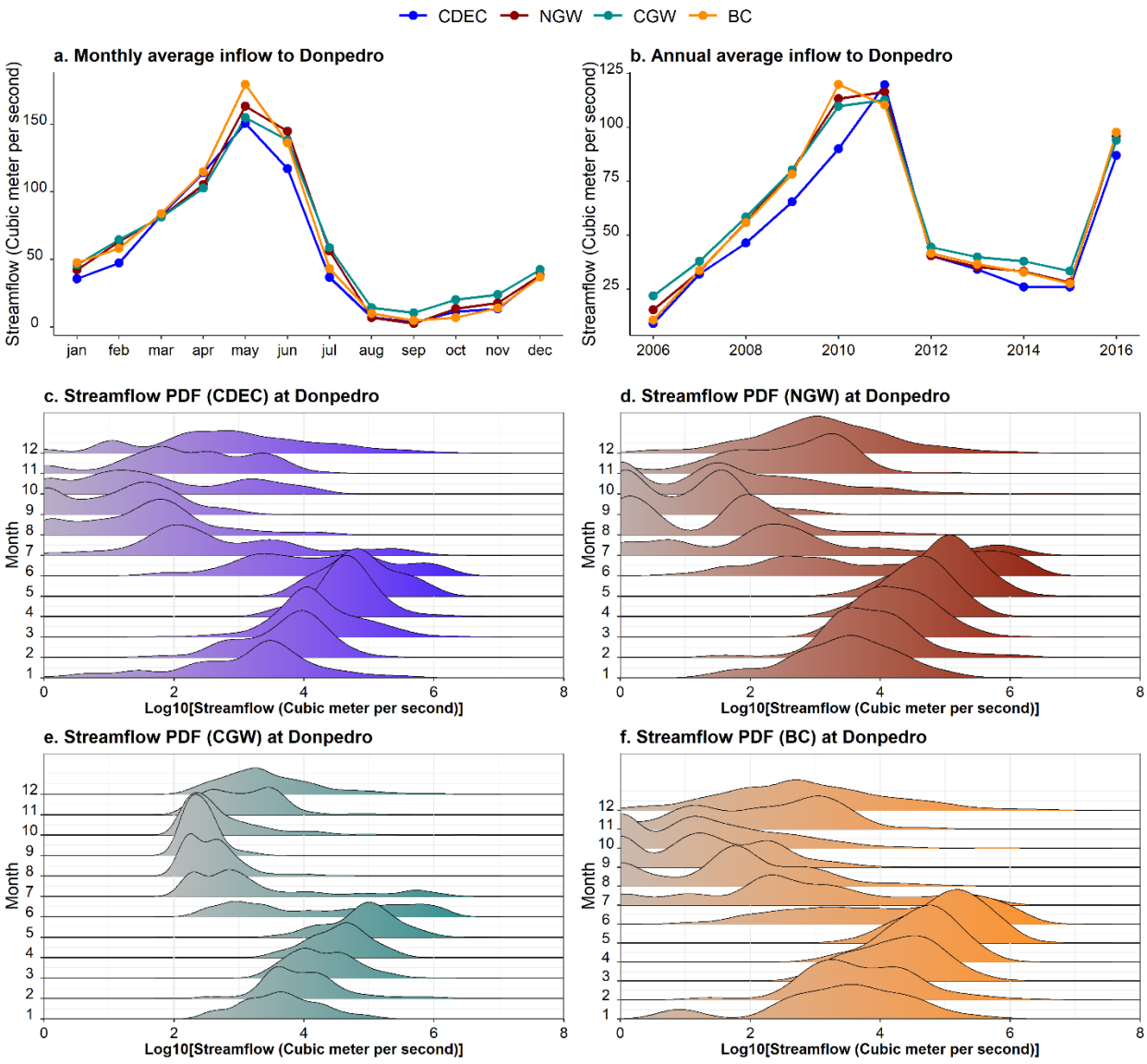


**Figure S11.** Comparison between the observed and simulated streamflow scenarios at Don Pedro Dam. The simulated streamflow scenarios include raw WRF-Noah-MP flow (NGW), WRF Noah-MP groundwater-corrected flow (CGW), and bias-corrected flow (BC). Panel a. and b. demonstrate the average monthly and average annual streamflow, respectively. Panel c., d., e., and f. show the monthly separated probability density function of daily streamflow for our four flow scenarios (observed, groundwater corrected, no groundwater correction, and bias-corrected).

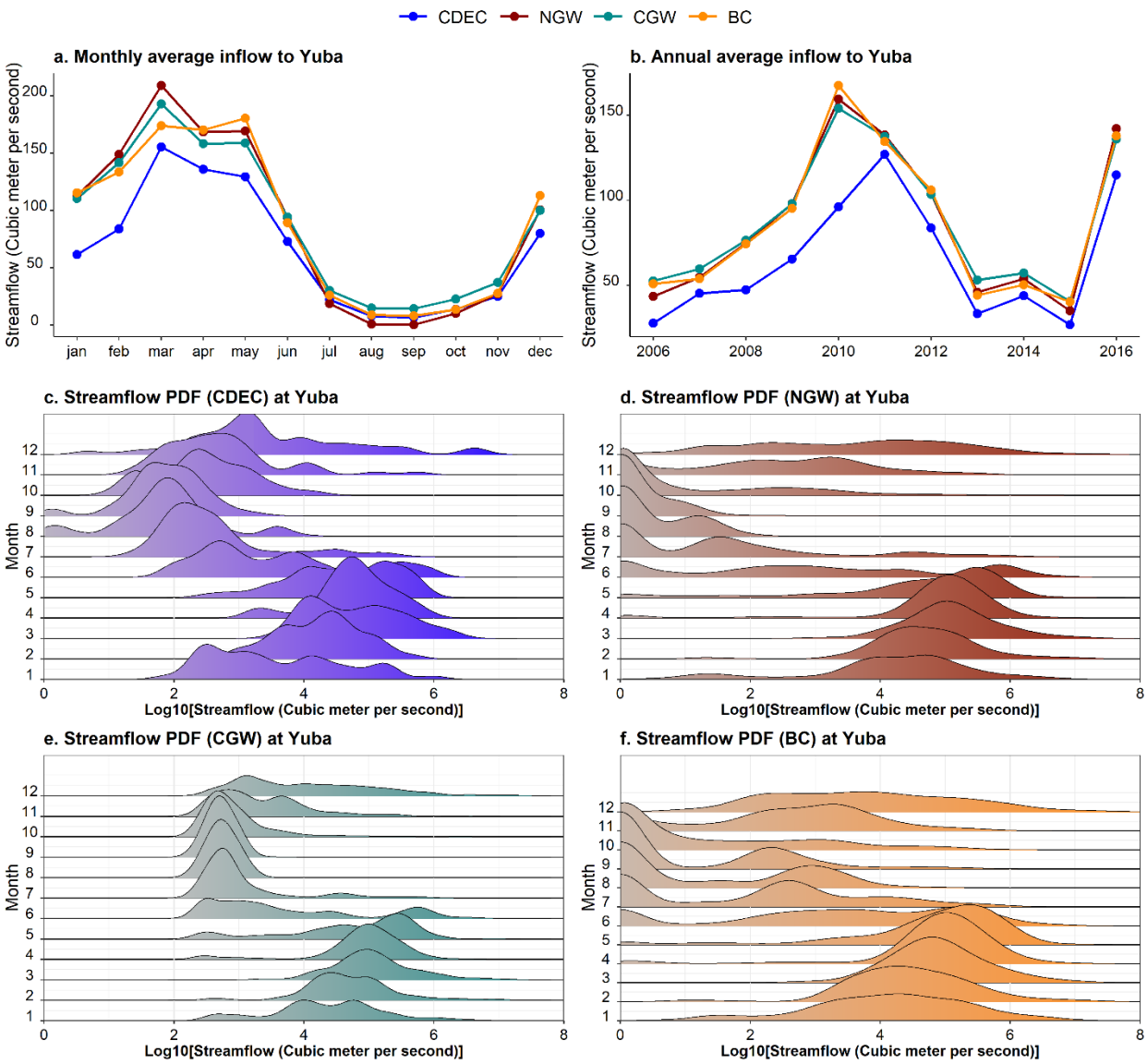


**Figure S12.** Comparison between the observed and simulated streamflow scenarios at Yuba Dam. The simulated streamflow scenarios include raw WRF-Noah-MP flow (NGW), WRF Noah-MP groundwater-corrected flow (CGW), and bias-corrected flow (BC). Panel a. and b. demonstrate the average monthly and average annual streamflow, respectively. Panel c., d., e., and f. show the monthly separated probability density function of daily streamflow for our four flow scenarios (observed, groundwater corrected, no groundwater correction, and bias-corrected).

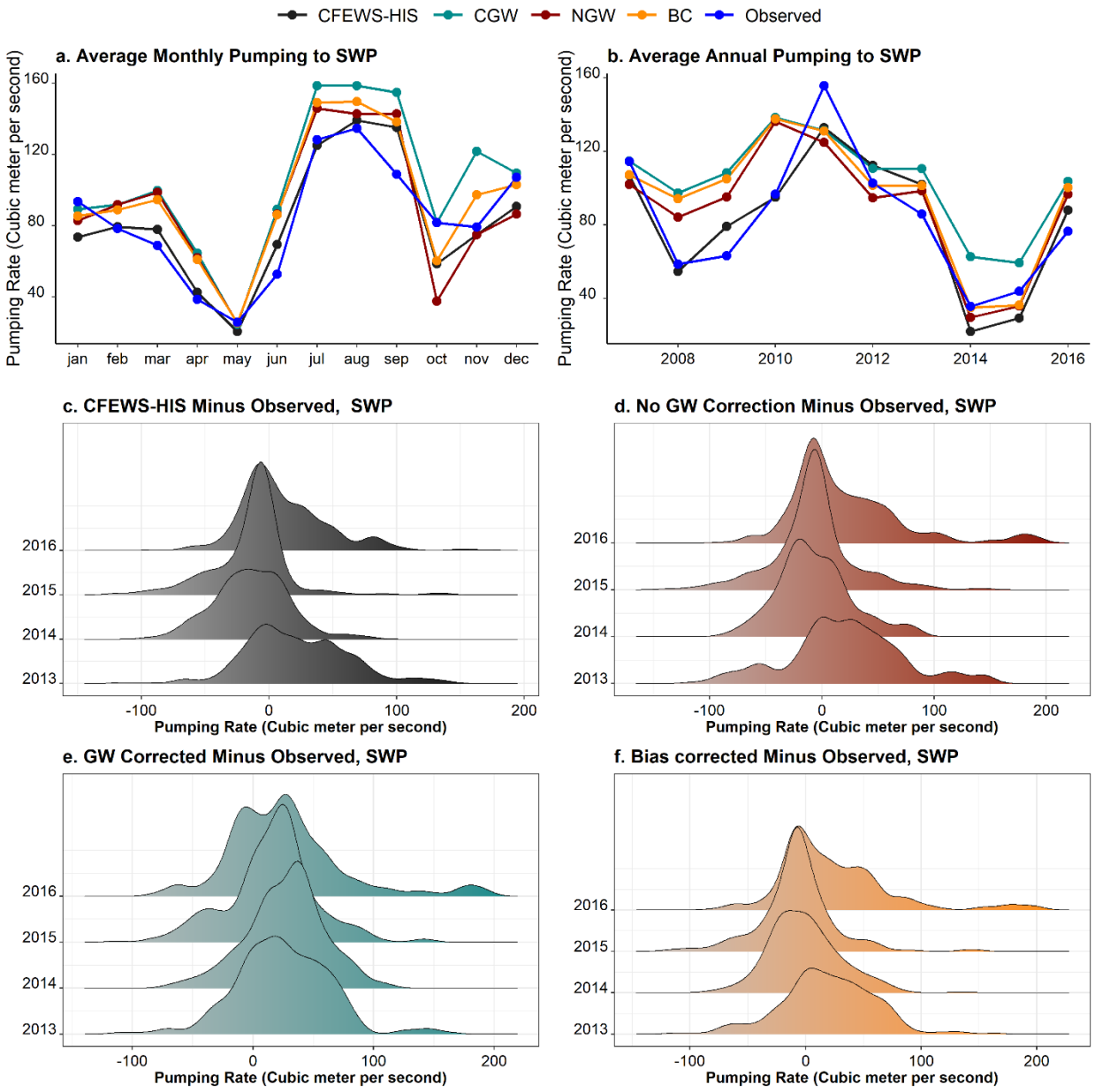


**Figure S13.** Pumping rate to State Water Project (SWP). This figure compares the observed pumping to SWP with simulations of CALFEWs under different streamflow scenarios (i.e., observed [CDEC], raw WRF-Noah-MP output [NGW], groundwater corrected [CGW], and bias-corrected [BC]). Panels a. and b. show average monthly and annual pumping rate to the SWP. Panels c., d., e., and f. show the probability density function of daily differences between recorded pumping to SWP and CALFEWs simulated pumping under the CDEC, NGW, CGW, and BC, respectively.

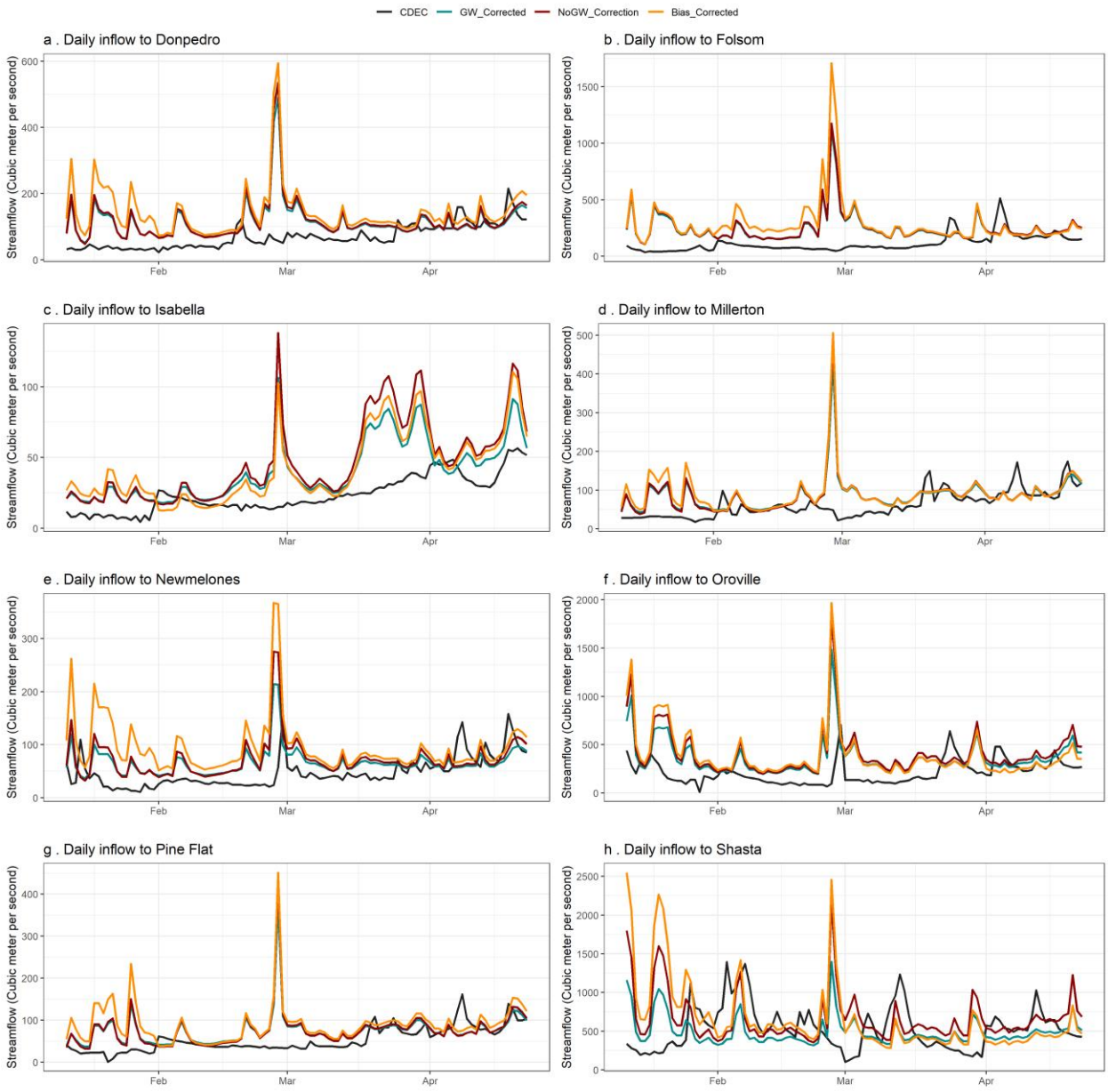


**Figure S14.** Streamflow input to different inflow points of CALFEWs during the Spring 2010. Our streamflow input scenarios include observed [CDEC], raw WRF-Noah-MP output [NGW], groundwater corrected [CGW], and bias-corrected [BC].

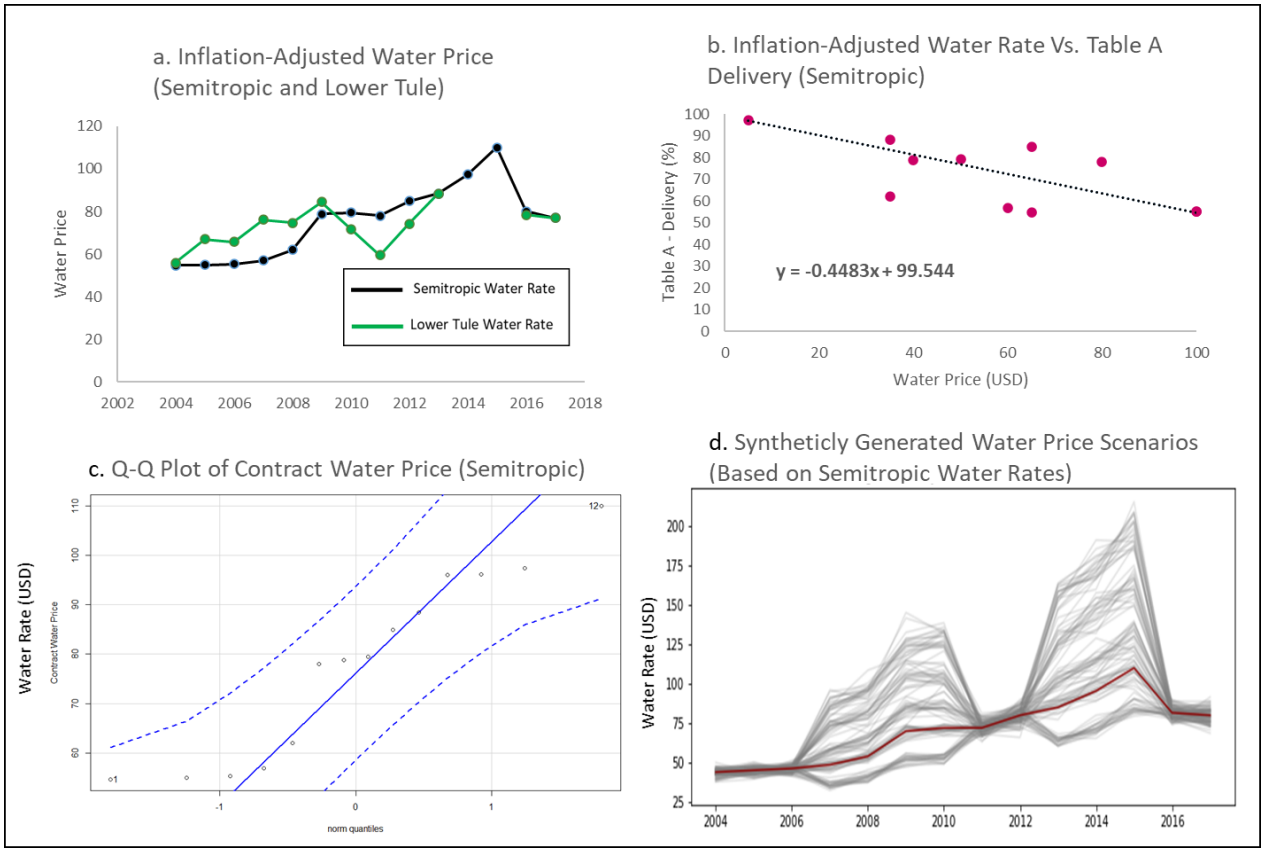


**Figure S15.** Synthetic generation of water price scenarios. Panel a shows one hundred synthetically generated water price scenarios based on contract water price data for the Lower Tule irrigation district. The stochastic abstraction of the mean and variability of pricing dynamics reflects a temporally consistent and plausible pricing of water. Panel b show the inflation adjusted contract water price data for the Lower Tule irrigation district. Panel c indicates how water price changes with SWP water delivery. Panel d shows the q-q plot of recorded water price with 95% confidence interval.

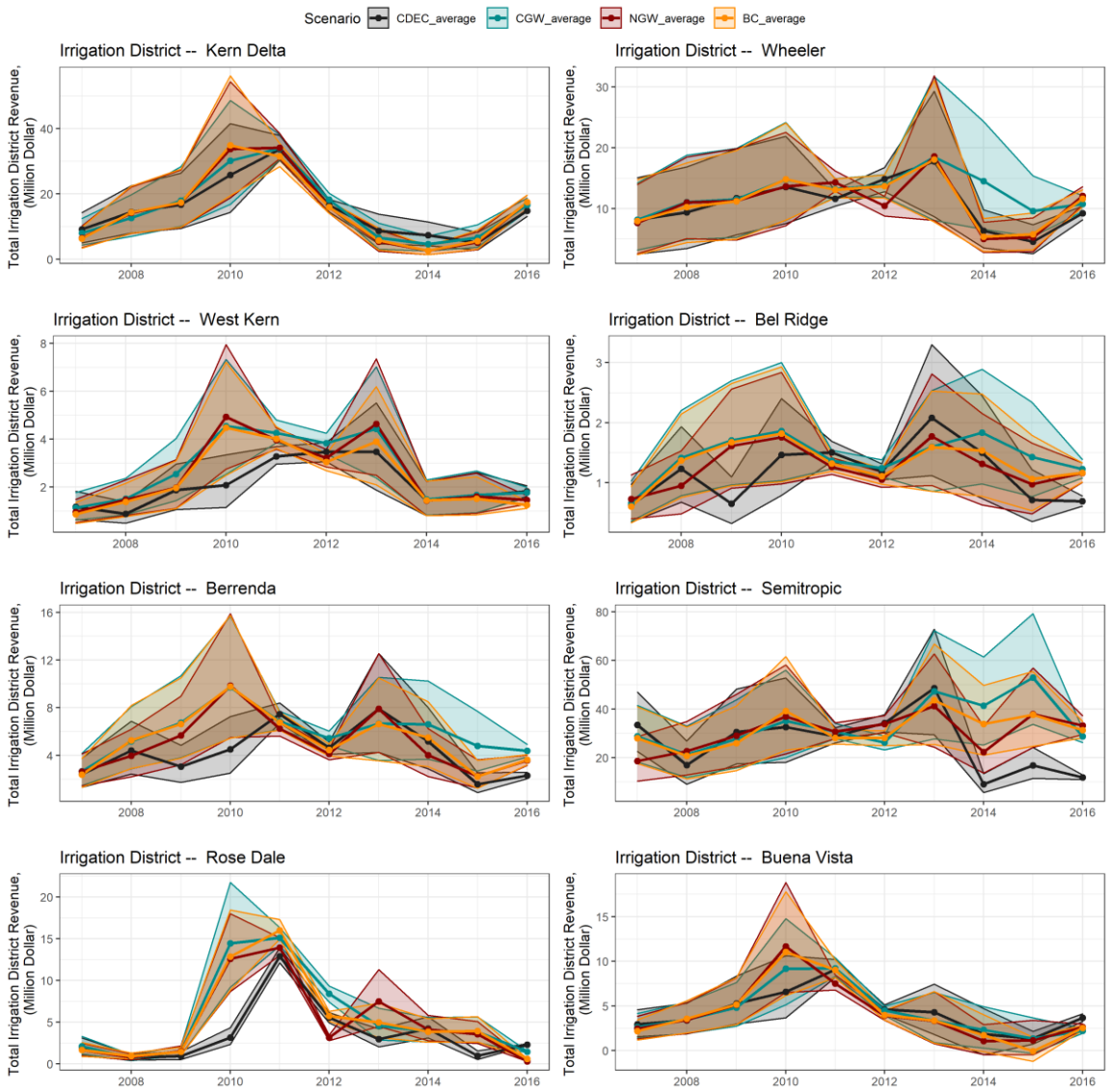


**Figure S16.** Annual revenue of irrigation districts considered in this study. The simulated streamflow scenarios include raw WRF-Noah-MP flow (NGW), WRF Noah-MP groundwater-corrected flow (CGW), and bias-corrected flow (BC). In this figure the uncertainty bounds are generated from our 100 water price realizations and the solid lines demonstrates the average of all those water price scenarios.

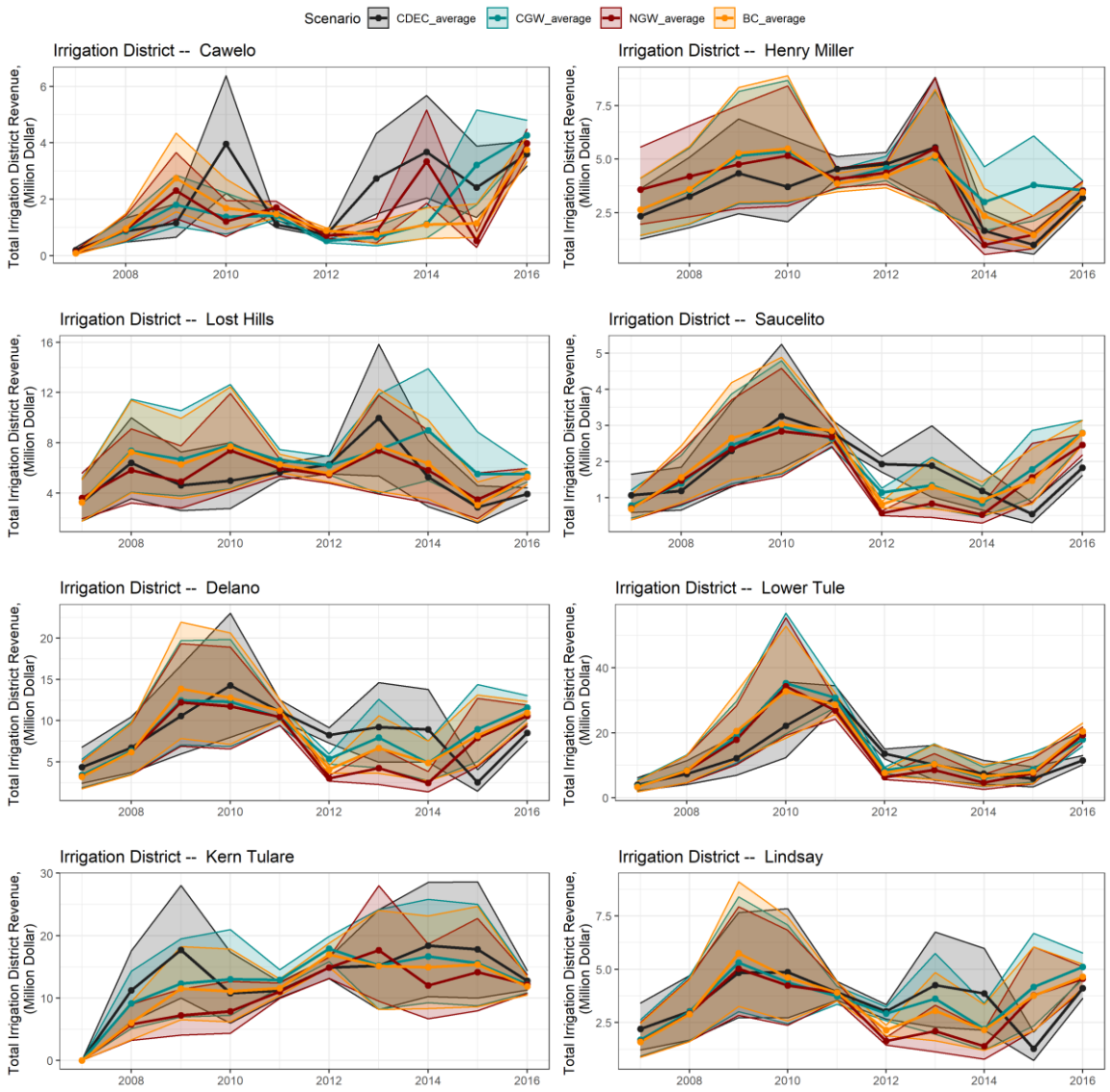


**Figure S17.** Annual revenue of irrigation districts considered in this study. The simulated streamflow scenarios include raw WRF-Noah-MP flow (NGW), WRF Noah-MP groundwater-corrected flow (CGW), and bias-corrected flow (BC). In this figure the uncertainty bounds are generated from our 100 water price realizations and the solid lines demonstrates the average of all those water price scenarios.

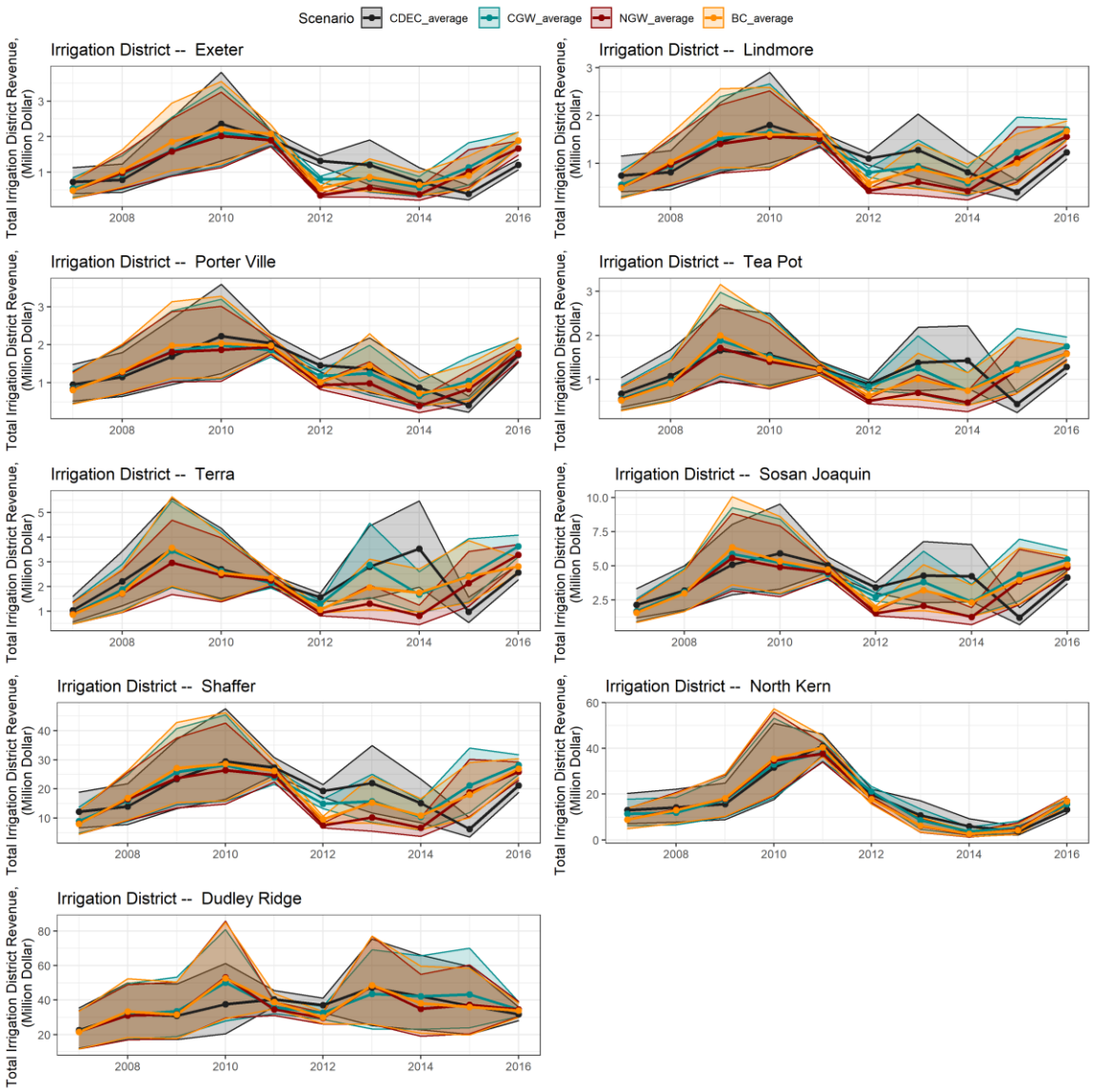


**Figure S18.** Annual revenue of irrigation districts considered in this study. The simulated streamflow scenarios include raw WRF-Noah-MP flow (NGW), WRF Noah-MP groundwater-corrected flow (CGW), and bias-corrected flow (BC). In this figure the uncertainty bounds are generated from our 100 water price realizations and the solid lines demonstrates the average of all those water price scenarios.

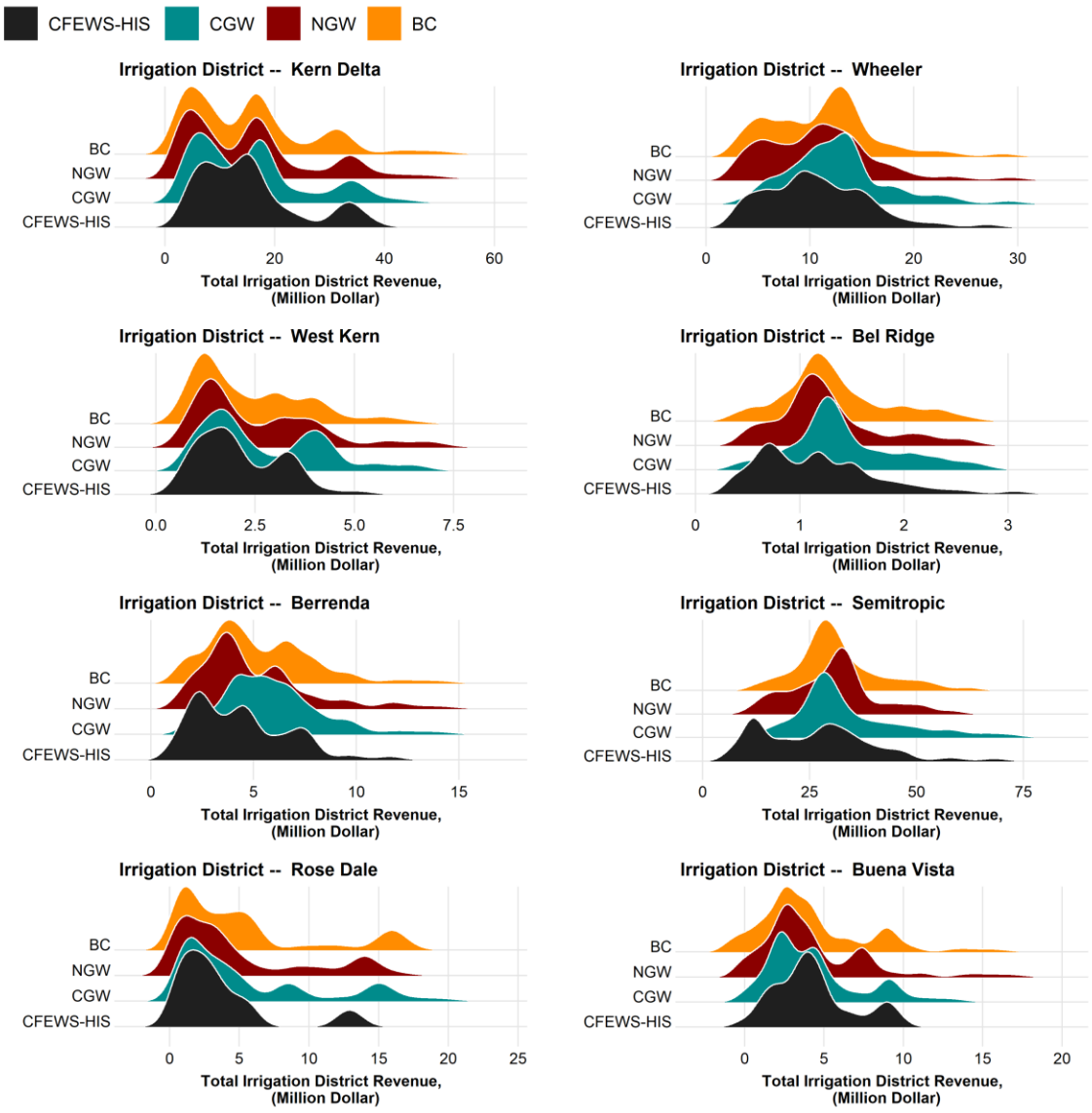


**Figure S19.** Annual revenue of irrigation districts considered in this study. The simulated streamflow scenarios include raw WRF-Noah-MP flow (NGW), WRF Noah-MP groundwater-corrected flow (CGW), and bias-corrected flow (BC). In this figure each probability distribution function includes one thousand data points representing combinations of the ten year simulation period and one hundred water price scenarios.

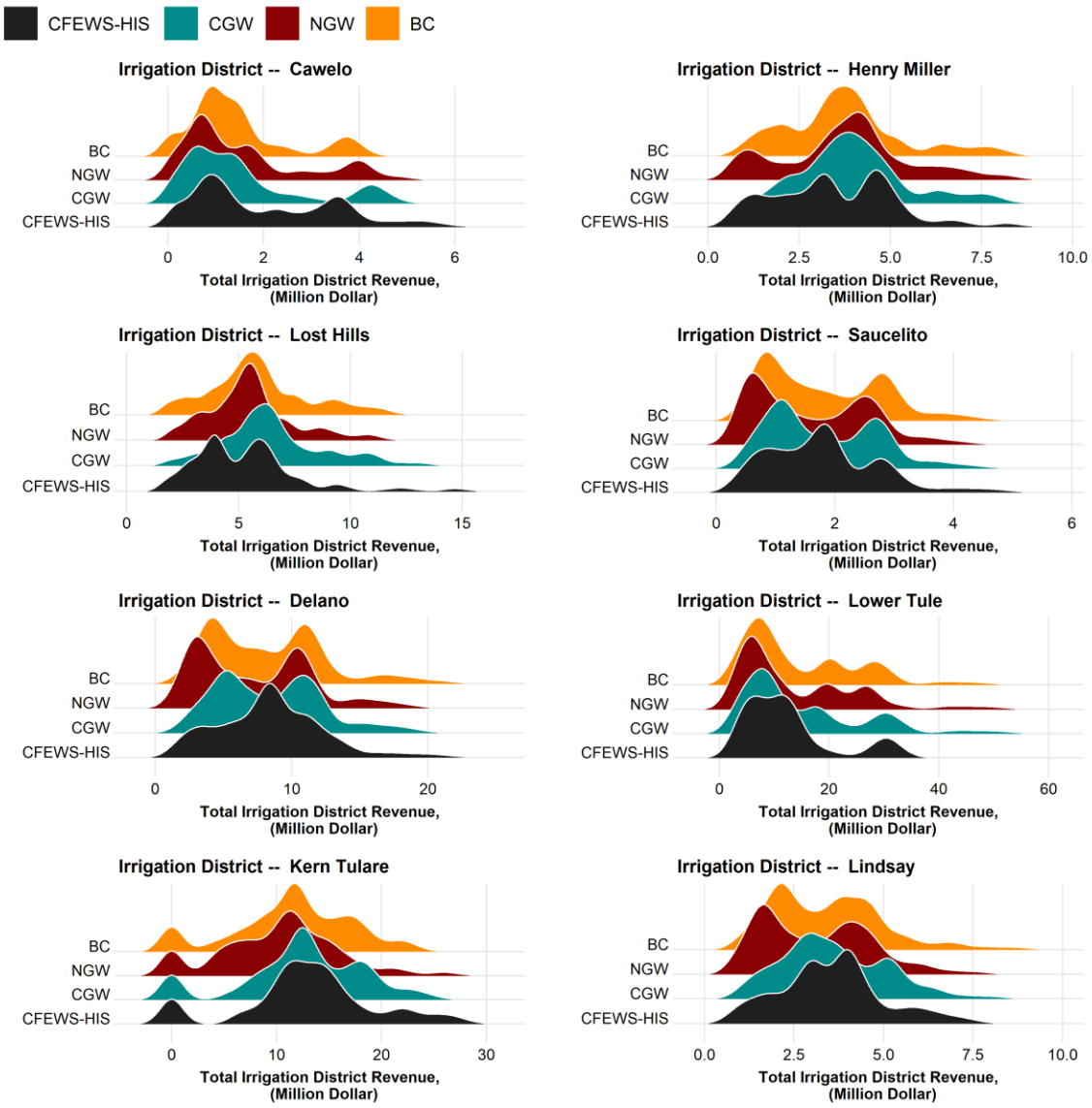


**Figure S20.** Annual revenue of irrigation districts considered in this study. The simulated streamflow scenarios include raw WRF-Noah-MP flow (NGW), WRF Noah-MP groundwater-corrected flow (CGW), and bias-corrected flow (BC). In this figure each probability distribution function includes one thousand data points representing combinations of the ten year simulation period and one hundred water price scenarios.

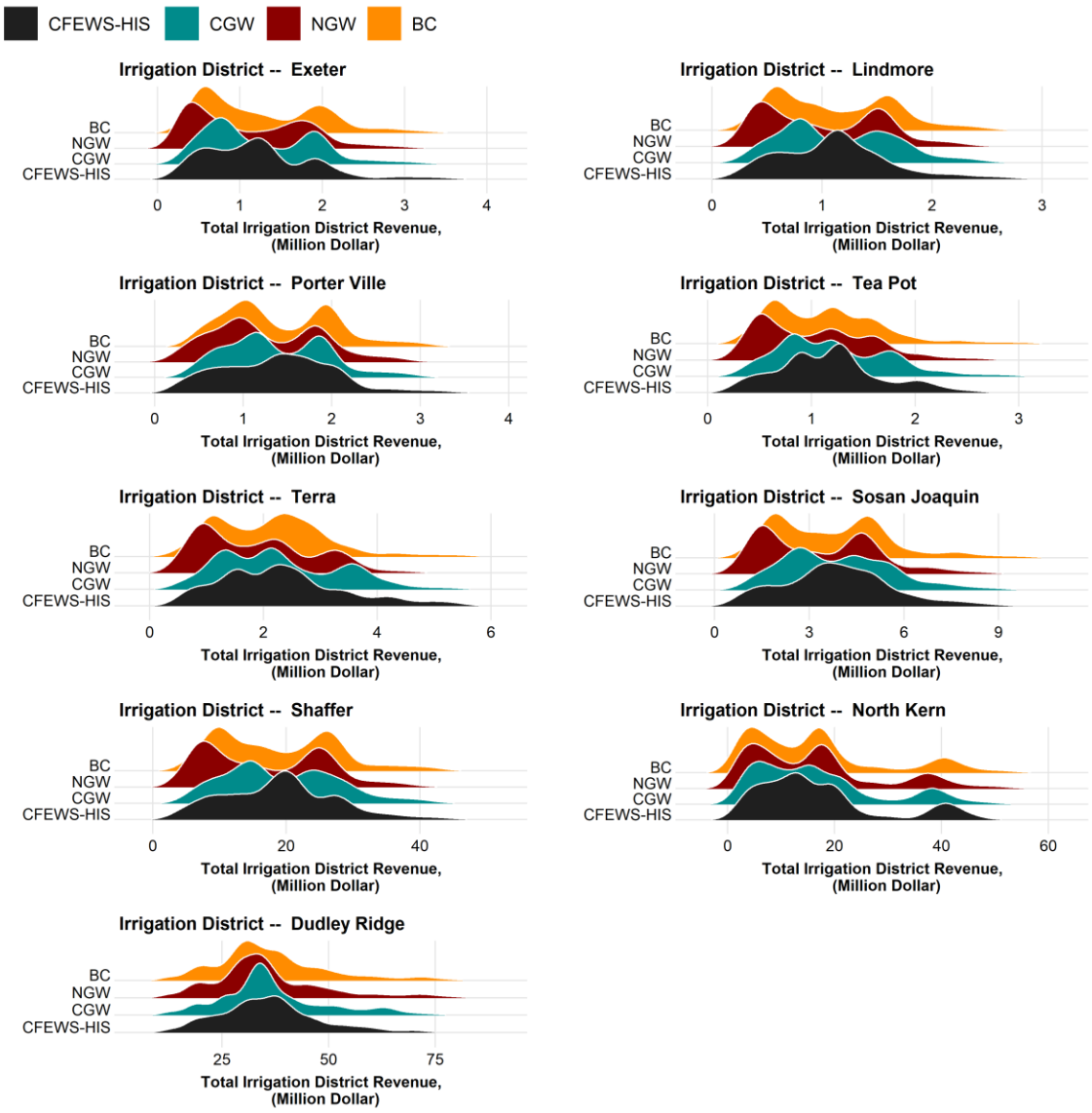


**Figure S21.** Annual revenue of irrigation districts considered in this study. The simulated streamflow scenarios include raw WRF-Noah-MP flow (NGW), WRF Noah-MP groundwater-corrected flow (CGW), and bias-corrected flow (BC). In this figure each probability distribution function includes one thousand data points representing combinations of the ten year simulation period and one hundred water price scenarios.

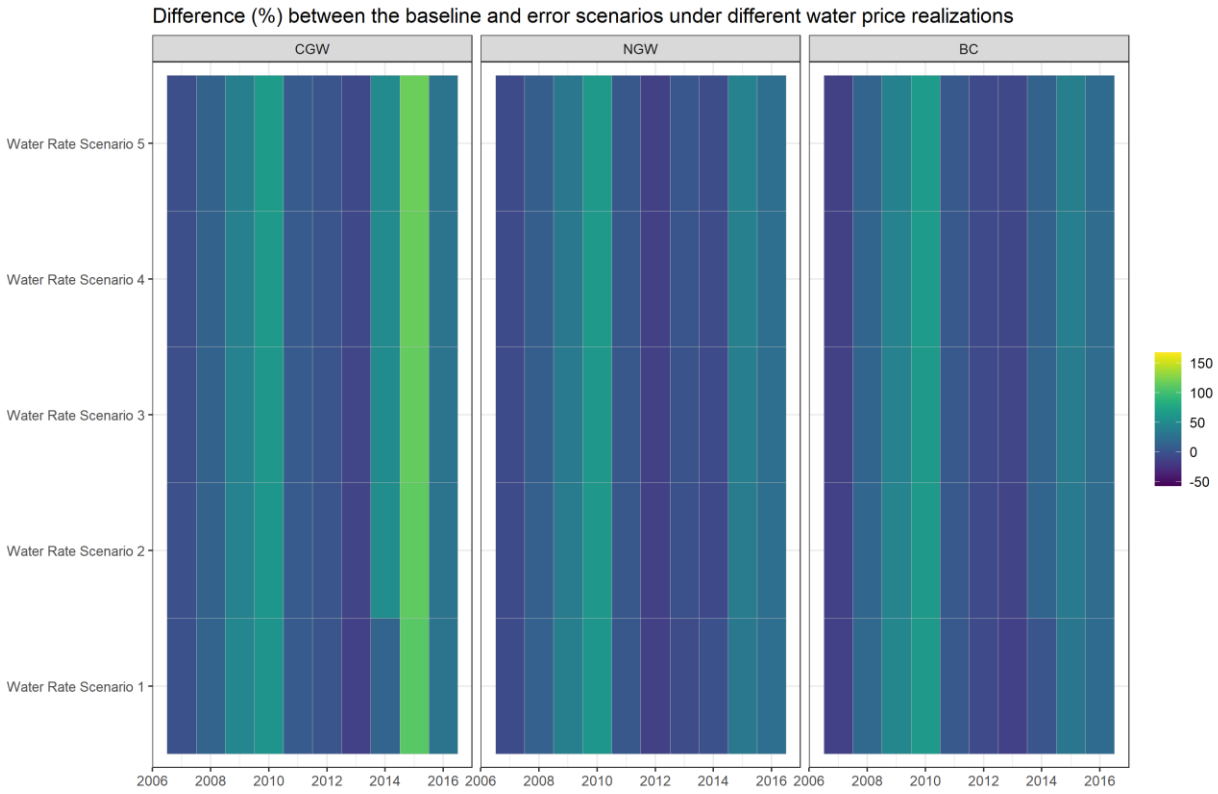


**Figure S22.** The difference between simulated state-wide irrigation district revenue under the baseline streamflow scenario (CFEWS-HIS) and simulate streamflow scenarios (i.e., raw WRF-Noah-MP flow (NGW), WRF Noah-MP groundwater-corrected flow (CGW), and bias-corrected flow (BC)). The differences are presented for each specific water rate scenario and each year. The percent differences are averaged over twenty water price realizations in each water rate scenario groups.

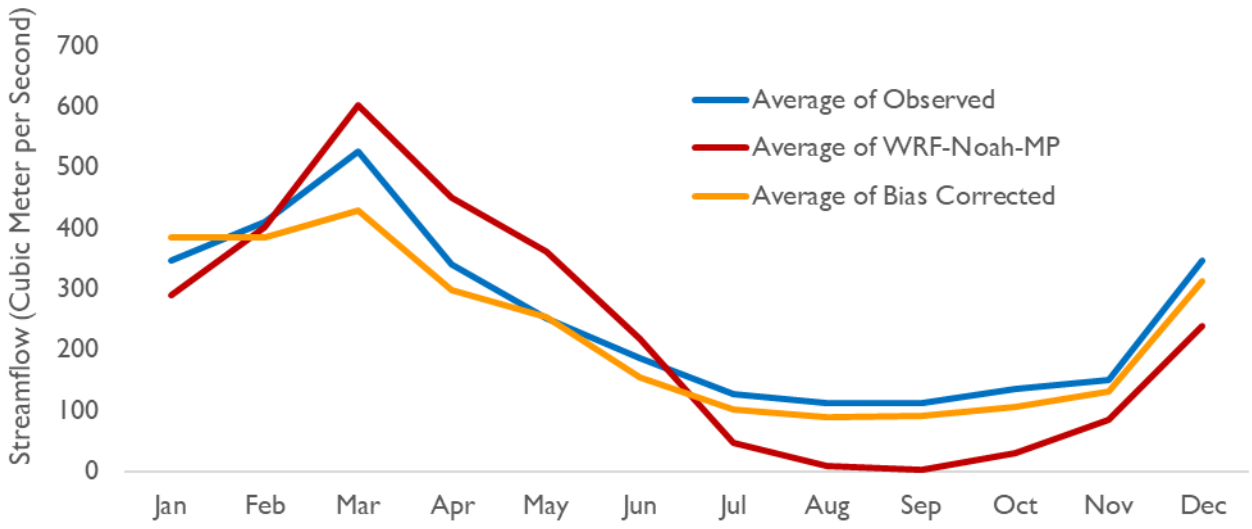


**Figure S23**. Impacts of quantile mapping bias correction on average monthly inflow to Shasta Dam. The streamflow scenarios to Shasta Dam include observed flow from CDEC, raw WRF-Noah-MP output [NGW], and bias-corrected [BC].

.

# Supplementary Tables

| | CFEW-HIS | CGW | NGW | BC |
|---|---|---|---|---|
| **Shasta** | 0.92 | 0.68 | 0.20 | 0.21 |
| **Oroville** | 0.95 | 0.00 | 0.52 | 0.08 |
| **Folsom** | 0.82 | 0.40 | 0.55 | 0.51 |
| **Yuba** | 0.79 | 0.18 | 0.45 | 0.27 |

**Table S1.** Observed dam storage vs. CALFEWs simulations. Nash-Sutcliffe Efficiency (NSE; Supplemental Materials 2) of recorded dam storage against CALFEWs simulations under different streamflow scenarios. Streamflow scenarios include: i) observed flow from California Department of Water Resources' Data Exchange Center (CFEW-HIS), ii) raw WRF-NoahMP (NGW), iii) groundwater corrected WRF-NoahMP (CGW), and iv) bias corrected WRF-NoahMP (BC).

| | CFEW-HIS | CGW | NGW | BC |
|---|---|---|---|---|
| **Shasta** | 0.75 | 0.41 | 0.06 | 0.47 |
| **Oroville** | 0.80 | -0.01 | -0.24 | -0.01 |
| **Folsom** | 0.87 | 0.32 | 0.28 | 0.22 |
| **Yuba** | 0.88 | -0.38 | -0.52 | -0.34 |

**Table S2.** Observed dam outflow vs. CALFEWs simulations. Nash-Sutcliffe Efficiency (NSE; Supplemental Materials 2) of recorded dam outflow against CALFEWs simulations under different streamflow scenarios. Streamflow scenarios include: i) observed flow from CDEC (CFEW-HIS), ii) raw WRF-NoahMP (NGW), iii) groundwater corrected WRF-NoahMP (CGW), and iv) bias corrected WRF-NoahMP (BC).

| Scenario | CFEW-HIS | CGW | NGW | BC |
|---|---|---|---|---|
| **CVP** | 0.601 | 0.091 | 0.034 | 0.304 |
| **SWP** | 0.683 | 0.323 | 0.257 | 0.363 |

**Table S3.** Observed pumping from delta vs. CALFEWs simulations. Performance metrics (Supplemental Materials 2) of the simulation of total annual pumping from the delta to the State Water Project (SWP) and the Central Valley Project (CVP). The simulated streamflow scenarios that were used to run CALFEWs include the baseline scenarios (CFEW-HIS), the groundwater-corrected WRF-Noah-MP output (CGW), the WRF-Noah-MP outputs with no groundwater correction (NGW), and bias-corrected WRF-Noah-MP streamflow (BC). In this table, ME, MAE, RMSE, and NSE stand for mean error, mean absolute error, root mean square error, and the Nash-Sutcliffe Efficiency, respectively.

| | BC | CGW | NGW | BC | CGW | NGW | BC | CGW | NGW |
|---|---|---|---|---|---|---|---|---|---|
| **Metrics** | **Don Pedro** | | | **Folsom** | | | **Isabella** | | |
| **ME** | 738.89 | 579.36 | 452.11 | 923.78 | 1201.02 | 1196.29 | 235.87 | 64.09 | 43.45 |
| **MAE** | 2205.51 | 2102.96 | 2120.00 | 3629.14 | 3488.00 | 3627.55 | 747.23 | 628.97 | 775.79 |
| **RMSE** | 4319.26 | 3984.47 | 4269.25 | 8405.65 | 7883.17 | 8188.98 | 1720.83 | 1498.23 | 1725.24 |
| **NSE** | 0.34 | 0.44 | 0.36 | -0.12 | 0.02 | -0.06 | 0.29 | 0.46 | 0.29 |
| | **Millerton** | | | **New Melones** | | | **Oroville** | | |
| **ME** | 689.08 | 214.82 | 199.63 | 414.18 | 349.08 | 251.39 | 1484.95 | 1818.39 | 1464.78 |
| **MAE** | 1865.41 | 1578.95 | 1742.77 | 1406.53 | 1252.14 | 1299.65 | 6794.44 | 5410.92 | 6966.59 |
| **RMSE** | 3519.75 | 2825.75 | 3246.54 | 2842.87 | 2156.47 | 2637.21 | 15337.19 | 13320.98 | 15689.85 |
| **NSE** | 0.45 | 0.65 | 0.54 | 0.20 | 0.54 | 0.31 | -0.51 | -0.14 | -0.58 |
| | **Pine Flat** | | | **Shasta** | | | **Yuba** | | |
| **ME** | 503.22 | 157.28 | 129.35 | 3575.26 | -1142.24 | -1824.35 | 656.17 | 1631.16 | 1536.91 |
| **MAE** | 1830.31 | 1652.31 | 1800.01 | 14249.78 | 8403.02 | 12750.50 | 3355.17 | 3317.23 | 3644.80 |
| **RMSE** | 3637.15 | 3227.05 | 3735.67 | 30799.27 | 20893.84 | 25053.60 | 7469.75 | 7163.67 | 8128.50 |

| | | | | | | | | | |
|---|---|---|---|---|---|---|---|---|---|
| **NSE** | 0.48 | 0.59 | 0.45 | -0.91 | 0.12 | -0.26 | -0.27 | -0.17 | -0.51 |

**Table S4.** Performance metrics of WRF-Noah-MP and bias corrected streamflow scenarios. Error metrics (Supplemental Materials 6) associated with the comparison of observed flow (from California Department of Water Resources' Data Exchange Center; CDEC) and the simulation of two WRF-Noah-MP streamflow scenarios: i) groundwater-corrected WRF-Noah-MP streamflow (CGW); ii) WRF-Noah-MP streamflow outputs with no groundwater correction (NGW); iii) bias-corrected WRF-Noah-MP streamflow (BC);. In this table, ME, MAE, RMSE, and NSE stand for mean error, mean absolute error, root mean square error, and the Nash-Sutcliffe Efficiency, respectively.

| | **Buena Vista** | | | **Wonderful** | | |
|---|---|---|---|---|---|---|
| **Metrics** | CGW | NGW | BC | CGW | NGW | BC |
| **ME** | -0.03 | 0.55 | 0.64 | 4.19 | 5.63 | 4.65 |
| **MAE** | 3.24 | 3.42 | 3.49 | 6.51 | 7.33 | 7.59 |
| **RMSE** | 9.59 | 9.61 | 9.97 | 11.63 | 11.88 | 12.29 |
| **NSE** | 0.3 | 0.3 | 0.24 | 0.63 | 0.62 | 0.59 |

**Table S5.** Performance metrics (Supplemental Materials 6) of the simulation of groundwater withdrawals associated with two simulated streamflow scenarios (i.e., groundwater corrected, CGW; no groundwater correction, NGW; and bias corrected, BC). In this table, ME, MAE, RMSE, and NSE stand for mean error, mean absolute error, root mean square error, and the Nash-Sutcliffe Efficiency, respectively. The two irrigation districts considered in this section are Buena and Henry Miller.

| **District Name** | **Basin** | **Approximated location in Tulare basin** | **Water Delivery Project** | **Local Water Sources** |
|---|---|---|---|---|
| **Berrenda Mesa Irrigation District** | Tulare | West | SWP Delta | |
| **Belridge Irrigation District** | Tulare | West | SWP Delta | |
| **Buena Vista Irrigation District** | Tulare | West | SWP Delta | Kern River |

| | | | | |
|---|---|---|---|---|
| **Cawelo Irrigation District** | Tulare | Center | SWP Delta | Kern River |
| **Henry Miller Irrigation District** | Tulare | West | SWP Delta | |
| **Kern Delta Irrigation District** | Tulare | Center | SWP Delta | Kern River |
| **Lost Hills Irrigation District** | Tulare | West | SWP Delta | |
| **Rosedale-Rio Bravo District** | Tulare | Center | SWP Delta | Kern River |
| **Semitropic Water Storage District** | Tulare | West | SWP Delta | |
| **West Kern Irrigation District** | Tulare | West | SWP Delta | |
| **Wheeler Ridge-Maricopa District** | Tulare | West | SWP Delta | |
| **North Kern Irrigation District** | Tulare | East | | Kern River |
| **Delano-Earlimart Irrigation District** | Tulare | East | Friant | |
| **Exeter Irrigation District** | Tulare | East | Friant | |
| **Kern-Tulare Irrigation District** | Tulare | East | Friant | Cross Valley |
| **Lindmore Irrigation District** | Tulare | East | Friant | |
| **Lindsay-Strathmore Irrigation District** | Tulare | East | Friant | |
| **Lower Tule Irrigation District** | Tulare | East | Friant | Cross valley and Tule River |
| **Porterville Irrigation District** | Tulare | East | Friant | Tule River |
| **Saucelito Irrigation District** | Tulare | East | Friant | |
| **Shaffer-Wasco Irrigation District** | Tulare | East | Friant | |
| **Southern San Joaquin Irrigation District** | Tulare | East | Friant | |
| **Teapot Dome Irrigation District** | Tulare | East | Friant | |
| **Terra Bella Irrigation District** | Tulare | East | Friant | |
| **Dudley Ridge Irrigation District** | Tulare | West | SWP Delta | |

**Table S6.** Some of the general characteristics of the irrigation districts simulated in this study.

**References**


Cannon, A. J. (2018). "Multivariate quantile mapping bias correction: an N-dimensional probability density function transform for climate model simulations of multiple variables." *Climate Dynamics*, 50(1), 31–49.

Cannon, A. J., Sobie, S. R., and Murdock, T. Q. (2015). "Bias Correction of GCM Precipitation by Quantile Mapping: How Well Do Methods Preserve Changes in Quantiles and Extremes?" *Journal of Climate*, American Meteorological Society, 28(17), 6938–6959.

Donnelly, K., and Christian-Smith, J. (2013). "An Overview of the 'New Normal' and Water Rate Basics." *Pacific Institute, Oakland, Calif*.

François, B., Vrac, M., Cannon, A. J., Robin, Y., and Allard, D. (2020). "Multivariate bias corrections of climate simulations: which benefits for which losses?" *Earth System Dynamics*, Copernicus GmbH, 11(2), 537–562.

Gudmundsson, L., Bremnes, J. B., Haugen, J. E., and Engen-Skaugen, T. (2012). "Technical Note: Downscaling RCM precipitation to the station scale using statistical transformations – a comparison of methods." *Hydrology and Earth System Sciences*, 16(9), 3383–3390.

Gupta, H. V., Sorooshian, S., and Yapo, P. O. (1998). "Toward improved calibration of hydrologic models: Multiple and noncommensurable measures of information." *Water Resources Research*, 34(4), 751–763.

Gupta, H. V., Wagener, T., and Liu, Y. (2008). "Reconciling theory with observations: elements of a diagnostic approach to model evaluation." *Hydrological Processes*, 22(18), 3802–3813.

Hamlet, A., and Lettenmaier, D. (1999). "Columbia River Streamflow Forecasting Based on ENSO and PDO Climate Signals." *Journal of Water Resources Planning and Management*, 125(6), 333–341.

Hawkins, E., Osborne, T. M., Ho, C. K., and Challinor, A. J. (2013). "Calibration and bias correction of climate projections for crop modelling: An idealised case study over Europe." *Agricultural and Forest Meteorology*, Agricultural prediction using climate model ensembles, 170, 19–31.

Howitt, R., Medellín-Azuara, J., MacEwan, D., Lund, J., and Sumner, D. (2014). *Economic Analysis of the 2014 Drought for California Agriculture*. CCenter for Watershed Sciences, University of California, Davisenter for Watershed Sciences, 20.

Luo, M., Liu, T., Meng, F., Duan, Y., Frankl, A., Bao, A., and De Maeyer, P. (2018). "Comparing Bias Correction Methods Used in Downscaling Precipitation and Temperature from Regional Climate Models: A Case Study from the Kaidu River Basin in Western China." *Water*, Multidisciplinary Digital Publishing Institute, 10(8), 1046.

Maraun, D. (2013). "Bias Correction, Quantile Mapping, and Downscaling: Revisiting the Inflation Issue." *Journal of Climate*, 26(6), 2137–2143.

Medellín-Azuara, J., Vergati, J. A., Sumner, D. A., Howitt, R. E., and Lund, J. R. (2012). *Analysis of effects of reduced supply of water on agricultural production and*

*irrigation water use in Southern California*. Working paper. University of California Agricultural Issues Center.

Mishra, V., Bhatia, U., and Tiwari, A. D. (2020). "Bias-corrected climate projections for South Asia from Coupled Model Intercomparison Project-6." *Scientific Data*, 7(1), 338.

Mitchell, D., Hanak, E., Baerenklau, K., Escriva-Bou, A., McCann, H., Pérez-Urdiales, M., and Schwabe, K. (2017). "Building drought resilience in California's cities and suburbs." *Public Policy Institute of California*, 1–49.

Moallemi, E. A., Kwakkel, J., de Haan, F. J., and Bryan, B. A. (2020). "Exploratory modeling for analyzing coupled human-natural systems under uncertainty." *Global Environmental Change*, 65, 102186.

Nash, J. E., and Sutcliffe, J. V. (1970). "River flow forecasting through conceptual models part I — A discussion of principles." *Journal of Hydrology*, 10(3), 282–290.

Oreskes, N., Shrader-Frechette, K., and Belitz, K. (1994). "Verification, Validation, and Confirmation of Numerical Models in the Earth Sciences." *Science*, American Association for the Advancement of Science, 263(5147), 641–646.

Piani, C., Haerter, J. O., and Coppola, E. (2010). "Statistical bias correction for daily precipitation in regional climate models over Europe." *Theoretical and Applied Climatology*, 99(1), 187–192.

Wallis-Lage, C., and Chevrette, J. (2012). "Strategic directions in the US water utility industry." *Journal (American Water Works Association)*, JSTOR, 104(8), 73–83.

Wichelns, D. (2010). "Agricultural Water Pricing: United States." OECD.

Zeff, H., Hamilton, A. L., Malek, K., Herman, J. D., Cohen, J. S., Medellin-Azuara, J., Reed, P. M., and Characklis, G. W. (2020). *California's Food-Energy-Water System: An Open Source Simulation Model of Adaptive Surface and Groundwater Management in the Central Valley*. engrXiv.